# Experimental assessment of the similarity law for a one-dimensional coupled heat and water vapor diffusion in hemp concrete

A. Charaka, J. Berger, F. Benmahiddine, Rafik Belarbi

# Experimental assessment of the similarity law for a one-dimensional coupled heat and water vapor diffusion in hemp concrete

A.Charaka[1,2*], J.Berger[1], F.Benmahiddine[1,2], and R.Belarbi[1,2,3]

[1]LaSIE, UMR 7356 CNRS La Rochelle Université, Avenue Michel Crépeau, 17042, La Rochelle Cedex1, France
[2]4evLab, LaSIE, CNRS, EDF R&D, La Rochelle Université, Avenue Michel Crépeau, 17042, La Rochelle Cedex1, France
[3]Department of Architecture, Canadian University Dubai, City Walk, Dubai, United Arab Emirates
[*]Corresponding author: achraf.charaka@univ-lr.fr

2022

# Highlights

1. Similarity laws are verified in the framework of a one-dimensional heat and water vapor diffusion problem through an experimental campaign.
2. Two configurations of hemp concrete samples, equivalent in terms of similarity laws, are exposed to thermal and hydric stress.
3. Temperature and relative humidity at equivalent positions in both samples are measured and compared.
4. A detailed uncertainty investigation is proposed to discuss the reliability of the observed discrepancies.
5. The comparison of discrepancies and entire uncertainties show a good agreement between the reference and reduced configurations.

# Abstract

Similarity law is a mathematical mapping that aims to set up equivalences between different configurations regarding the involved physical parameters, space dimensions and the duration of the configuration. These equivalences are defined by means of the dimensionless formulation of the physical model that describes a phenomenon. This concept is widely adopted in some scientific fields, notably in computational fluid dynamics. In heat and water vapor diffusion, similarities are applicable theoretically on configurations distinct in terms of material, space dimensions, duration or even imposed stress magnitude. It is worth noting that these are slow kinetic phenomena. In this regard, this study aims to verify similarities experimentally while using hemp concrete and reducing the duration of a reference experiment. Before performing measurements, two main limitations are fixed. First, by means of an experimental design, heat and moisture transfer are assumed one-dimensional. In addition, Dirichlet boundary conditions are considered at the surface that is exposed to ambient air. Mainly, temperature and relative humidity are measured at the quarter and middle of the material in order to compare the two similar configurations. Afterwards, an uncertainty study is carried out in order to discuss and justify the observed discrepancies. Following a deterministic approach, this investigation considers five sub-uncertainties which are related to : the calibration of used sensors, their positions, time of response, randomness of an experiment and the boundary condition modeling. Results show a good agreement between the reference and reduced configurations. Indeed, the discrepancies between both are entirely within the calculated confidence intervals.

# Keywords

heat conduction and water vapor diffusion, similarity analysis, porous material, experimental bench-marking, uncertainty quantification.

# 1 Introduction

Worldwide, the building sector is responsible for a consumption of 44 % of global energy. A significant part of building losses is due to the behavior of the envelope. Therefore, a decrease

in the energy consumption of a building relies partially on the understanding of interactions between building outdoor walls and external environment, specifically for recently introduced bio-based materials. Explicitly, studies on thermal and water vapor diffusion through construction materials, highlight the necessity of considering the thermal and hydric response of a building in regard to variable climate stress. These phenomena are highly coupled and governed by second order differential equations which are derived from heat and water amount conservation formula [1]. Moreover, these diffusion are complex phenomena that occur slowly, especially the one of water vapor. The slow kinetic is related to the nature of moisture diffusion which is a transport phenomenon, where water can migrate only trough open pore networks in liquid and vapor forms. The tortuosity of a material, which is a property defining the complexity of its micro-structure, influences as well water transport. In this respect, a bio-based material is known by a high heterogeneity and micro-structure complexity as a composite media. Based on the latter, it is important noting that the long kinetic of heat and water vapor diffusion represents a serious experimental issue, which should be faced.

The hygrothermal behavior of construction materials is widely investigated using approaches based on experimental designs and numerical simulations. Some of the references cited in the literature review carried in [2] can be mentioned specifically. According to [3], the study provides data-sets for validating one-dimensional heat and moisture diffusion models step by step, gradually increasing the complexity of a multi-layer wall with hygroscopic components and using variable climate stress. Furthermore, the influence of sorption curves dependence on temperature is investigated on the hygrothermal behavior of hemp concrete [4]. Another study [5] highlights the experimental characterization of moisture, heat, physical and mechanical properties of a recycled expanded polystyrene mortar. The experimental characterization is conducted also on a cement paste in order to evaluate the insulator adding impact. Afterwards, numerical results are compared to a 85-day experiment in[6]. Generally, these works involve experiments which aim either to confront numerical models of heat and water vapor diffusion or to propose a data set serving as bench-marking. However, these studies analyze the diffusion phenomena during short periods. A more meaningful and challenging approach would be to perform long-term experiments (years) to discuss further the hygrothermal behavior of porous materials.

One of the solutions would be the use of similarities. It aims to set an equivalence between two or more distinct configurations. This mapping relies on the scaling of the model that is used for a theoretical prediction of a studied phenomenon. Afterwards, the equivalence is defined based on a set of dimensionless numbers, each describes generally an aspect that is associated to the phenomenon. For example, a study [7] analyzes the use of dimensionless numbers, such as the Buningham and plastic ones, in the context of viscoplastic materials. According to the latter, some number sets are preferable to others in order to explore the solution space. Generally, similarity is helpful in diverse scientific fields [8] such as structure resistance, computational fluid dynamics, acoustics, aerodynamics, ocean engineering [9] and mechanics. In fluid dynamics for example, the purpose is mainly to compare several fluid flows thanks to a set of dimensionless numbers. The authors in [10, 11] established a similarity theory for heat transfer at super-critical pressures in order to find similar phenomenological behaviors while considering different fluids. In addition, a scale analysis was carried out to develop relationships among physical and geometrical parameters for two types of coil cavity receivers [12]. Herein, the effects of scaling on the performance of a solar receiver is addressed in order to discuss the

possibility of extending small designs to large-scale models. Moreover a study, from a different scientific field, proposes a method to relate models and prototype made with different materials, while considering small thickness distortions [13]. This approach is useful to evaluate the behavior of a plate structure against impulsive loading. In addition, similarity is applied to study the acoustic radiation of flat orthotropic flexural panels [14]. The paper assesses the validity of similarity on rectangular panels radiating sound in a semi-infinite light fluid medium. As for aero and hydrodynamics, large structures such as aircraft or wind turbines are pre-studied on a small scale [15, 16] and then designed using similarities. Subsequently, a similarity law of flow rate for ventilated hot-gas super cavity flows is found and described in [17]. The originality lied on water phase changes, whose effects were evaluated on similarity and the modeling scheme. Following another study [18], similarity is investigated on external flow field and internal heat transfer. Particularly, the law is verified by proposing a real aircraft and its scaled models. The results showed a good agreement between the scaled model and the real aircraft. Moreover, a dynamic similarity theory is introduced into a gear transmission system [19]. Particularly, the scale model is designed for the dynamic response. Thereafter, it is validated by free and forced vibration response. Authors in [20] carried simulations and a similarity model test to investigate the failure mechanism of a rock mass around the mined-out area above the high way tunnel. A law is revealed which could be significant for guiding similar engineering constructions.

In addition, heat and moisture diffusion through construction porous materials is a field where, to our best knowledge, a few works used similarity laws. In this respect, an annual moisture variation in a building wall is studied under a mild climate, employing a small-scale model and similarity [21]. In this investigation, an experimental design is proposed, using a wall small-scale model and similarity laws which are based on heat and moisture diffusion equations. Similarity is used to confront numerical results (standard configuration) to those of an experiment, which is an equivalent small-scale model. Lastly, the experimental validity of similarity is assessed for a heat conduction problem according to [22]. The study highlights the reliability of these laws on two similar experiments. For this purpose, temperatures inside materials are measured and confronted. First experiment (reference) lasts $72\,\mathsf{h}$ and the second (reduced) endures only $32\,\mathsf{h}$. Based on the good agreement of measurements, the utility of such laws to reduce the duration of long heat diffusion experiments is evidenced. Focusing always on heat and moisture diffusion investigations, a study [23] deals with similarity to assess these phenomena while considering 49 types of material. Similarity was obtained if the dimensionless numbers related to the problem were equal from one configuration to another. Therefore, all cited studies showed that similarities might have a significant role when addressing an experimental work to reduce its duration. Besides, it is important to underline that similarity is validated in the literature only for heat diffusion within porous construction materials.

The present work ensures a continuity of [22], and consists in extending the validity of similarity to a more general case. It proposes an experimental methodology that verifies the validity of similarity of a one-dimensional heat and moisture diffusion phenomena within porous building materials. In particular, the paper aims to verify the reliability of this law in maintaining the same results, between two configurations different in duration. The comparison is performed using measurements at similar positions and time instants. Resulting experimental discrepancies are quantified and discussed, based on the assessment of uncertainties. This step is meaningful since it is unknown whether a discrepancy is within the confidence range. Mostly,

an experimental similarity is reliable within a margin of error which can be interpreted by identifying the main constraints, hypotheses, and calculating the corresponding uncertainties.

The structure of this work is defined as follows. Section 2 proposes the physical model which is adopted to study heat and moisture diffusion in a porous material. In addition, it describes the dimensionless formulation of the problem, which will help defining the similarity laws. Afterwards, Section 3 presents the experimental facility that is used to assess the validity of an important assumption (Dirichlet condition modeling) as well as the reliability of similarity. Subsequently, Section 4 defines a detailed methodology to assess the propagation of uncertainty during a heat and moisture diffusion experiment. Thereafter, Section 5 highlights the results related to Dirichlet condition modeling assumption, both experiment uncertainty and the comparison of measurements in the standard and the reduced configuration. This section discusses additionally the experimental validity of similarity. Finally, a conclusion is given in Section 6 which suggests future investigations to improve the reliability of these laws.

# 2 Methodology

## 2.1 Assumptions of the study

Before defining the mathematical model that represents the coupled phenomena of heat and moisture diffusion, this section outlines the fixed assumptions for the remaining parts of this work.

**Assumption 1** *Heat and moisture diffusion are one-dimensional.*

**Assumption 2** *Heat and moisture boundary conditions at the surface are modeled according to* Dirichlet *type.*

**Assumption 3** *Material intrinsic properties do not depend on temperature.*

**Assumption 4** *The micro structure of the material are considered equals (from an averaged point of view) between two similar configurations. Thus, properties and their variation laws are considered the same for the two similar configurations.*

**Assumption 5** *The phenomenon of hysteresis is neglected and the variation of water content according to relative humidity is based on the averaged isotherm sorption curve.*

**Assumption 6** *Systematic uncertainty is constant and assumed independent of the location and the instant of a measurement.*

**Assumption 7** *The assessment of random uncertainties is approximated by using $N = 3$ samples in each configuration.*

Assumptions 1 and 2 have major importance in regards to the validation of similarity laws, so they will be discussed in the results.

## 2.2 Mathematical model

This part is dedicated to the definition of the equations that govern the coupled heat and moisture diffusion in porous media [24, 25]. The problem considered in this study follows a macroscopic approach based on the representative element volume [26]. In this respect, phenomena at the microscopic scale are averaged [27, 28] and convection is neglected due to low velocity fields in the pores of building materials and the size of these pores. Temperature $T\,[°\mathsf{C}]$ and vapor pressure $P_v\,[\mathsf{Pa}]$ are the driving potentials of this model. These two variables are strongly coupled and thus impact each other. The problem is written for a one-direction diffusion according to the Equations (1) and (2) :

$$C_m\,\rho\,\frac{\partial P_v}{\partial t} = \frac{\partial}{\partial x}\Big(\,(\,k_l + k_v\,)\,\frac{\partial P_v}{\partial x} + k_T\,\frac{\partial T}{\partial x}\,\Big) + \beta\,\frac{\partial T}{\partial t}\,, \tag{1}$$

$$C_p\,\rho\,\frac{\partial T}{\partial t} = \frac{\partial}{\partial x}\Big(\,(\,\lambda + h_l\,k_T\,)\,\frac{\partial T}{\partial x} + \alpha\,\frac{\partial P_v}{\partial x}\,\Big)\,, \tag{2}$$

Where $\rho\,[\mathsf{kg.m^{-3}}]$ designates the material density and is expressed as follows :

$$\rho = (1-n)\,\rho_s + n\,S_l\,\rho_l\,. \tag{3}$$

Where $n\,[-]$ is the porosity of the material, $\rho_s\,[\mathsf{kg.m^{-3}}]$ density of solid matrix, $S_l\,[-]$ the degree of saturation in water, $\rho_l\,[\mathsf{kg.m^{-3}}]$ water density. $C_p\,[\mathsf{J.kg^{-1}.K^{-1}}]$ is the global heat capacity. It is the combination of the specific heat of the material in the dry state $C_{ps}\,[\mathsf{J.kg^{-1}.K^{-1}}]$ and that of water in the pores of the medium $C_{pl}\,[\mathsf{J.kg^{-1}.K^{-1}}]$. It is expressed as follows :

$$C_p = \frac{(\,1-n\,)\,\rho_s\,C_{ps} + S_l\,n\,\rho_l\,C_{pl}}{(\,1-n\,)\,\rho_s + S_l\,n\,\rho_l}\,. \tag{4}$$

Furthermore, $C_m\,[\mathsf{Pa^{-1}}]$ represents the moisture storage capacity and is obtained via the isotherm adsorption and desorption curves. These curves illustrate the variation of water content $w\,[-]$ according to relative humidity $\phi\,[-]$ within the material and at a constant temperature [29]. Let assume that the variation of water content, according to relative humidity within the material, is determined at a constant temperature. On the other hand, it is also assumed that the sorption curve is obtained by averaging those of adsorption and desorption. The isotherm curve during the wetting and the drying of a porous material is not the same, this is due to the hysteresis phenomenon. The physical modification of the material, caused by water outflow, is responsible for this phenomenon. It is usually induced by the non-uniformity of pores geometry. In order to simplify the problem, this phenomenon will be neglected in the study assumption 5. Thus, the moisture storage capacity is defined as follows :

$$C_m\,(\,P_v\,,\,T\,) = \frac{1}{P_{sat}\,(\,T\,)}\,\frac{\partial w}{\partial \phi}\,. \tag{5}$$

Where $P_{sat}\,[\mathsf{Pa}]$ represent the saturation pressure and is given by Antoine's law as follows :

$$P_{sat}\,(\,T\,) = P^{\circ}_{sat}\,\left(\,\frac{T - T_c}{T_d}\,\right)^{p}\,, \qquad T \geq T_c\,, \tag{6}$$

Given that $P^{\circ}_{sat} = 997.3\,\mathsf{Pa}$, $T_c = 159.5\,\mathsf{K}$, $T_d = 120.6\,\mathsf{K}$ and $p = 8.275$. Afterwards, $k_v\,[\mathsf{s}]$ is water vapor permeability. It describes the transport of the water vapor form due to a vapor pressure gradient. This coefficient generally depends on water content and temperature. In this

case, it is assumed constant. In addition, Equation (1) introduces three other coefficients $k_l\,[\mathsf{s}]$, $k_T\,[\mathsf{kg.m^{-1}.s^{-1}.K^{-1}}]$ and $\beta\,[\mathsf{kg.m^{-3}.K^{-1}}]$. According to the model, they are defined as follows :

$$k_l\,(\,P_v\,,\,T\,) = \kappa_l\,\frac{R\,T\,\rho_l}{M\,P_v}\,. \tag{7}$$

$$k_T\,(\,P_v\,,\,T\,) = \frac{k_l\,R\,\rho_l}{M}\left(T\,\frac{\partial\,\ln\,\phi}{\partial T} + \ln\,\phi\right). \tag{8}$$

$$\beta\,(\,P_v\,,\,T\,) = \rho_s\,C_m\,\frac{P_v}{P_{sat}}\,\frac{\partial P_{sat}}{\partial T}\,. \tag{9}$$

Where $\kappa_l\,[\mathsf{s}]$ is the liquid conductivity. $R\,[\mathsf{J.mol^{-1}.K^{-1}}]$ is the ideal gas constant and the molar mass is given as $M\,[\mathsf{kg.mol^{-1}}]$. $k_T$ represent the moisture transport coefficient due to a temperature gradient. Furthermore, heat diffusion is primarily governed by the the material conduction that is defined by the coefficient $\lambda\,[\mathsf{W.m^{-1}.K^{-1}}]$. It generally depends on temperature and water content. However, this coefficient varies slightly with temperature. Therefore, only water content is considered in its expression, which is given below :

$$\lambda = n\,\lambda_l\,S_l + (1-n)\,\lambda_s\,. \tag{10}$$

Where $\lambda_s\,[\mathsf{W.m^{-1}.K^{-1}}]$ and $\lambda_l\,[\mathsf{W.m^{-1}.K^{-1}}]$ represent the material thermal conductivity at its dry state and the one of water. Note that Equation (10) underlines that the thermal conductivity of a porous material depends only on the saturation degree in water or water content in other words. It is worth noting that certain properties depend on temperature such as $\lambda$, $k_v$, $k_l$. However, unlike water content, these properties vary slowly according to temperature. In addition, the range of temperature variation is reduced in building physics, which is not the case in other scientific fields where temperature reaches higher thresholds. Hence, it is further considered that intrinsic properties do not vary according to temperature , which corresponds to the assumption 3. Moreover, $h_l\,[\mathsf{J.kg^{-1}}]$ is the water mass enthalpy. Notice that heat diffusion is also impacted by the presence of water within the open porous network. This fact is quantified by $\alpha\,[\mathsf{W.m^{-1}.Pa^{-1}}]$ which is a heat diffusion coefficient due to a vapor pressure gradient. Its expression is given as follows :

$$\alpha\,(\,P_v\,,\,T\,) = h_l\,(\,k_l + k_v\,) + L_v\,k_v\,.$$

$\alpha$ indicates the heat fraction transmitted as latent energy due to water vapor [30, 31]. This is evidenced via the water vapor permeability $k_v$ and the latent heat of vaporization $L_v$.

The upcoming study is carried out based on two hypotheses. On the one hand, the diffusion is considered one-dimensional along the $x$-axis for example. This is the first model assumption. It is possible to approximate the uni-directional flux condition. This is achieved by imposing a high thermal or moisture resistance along other diffusion directions. Materials with low thermal conductivity or water vapor permeability help limiting heat and moisture diffusion. Moreover, this assumption can also be approximated by considering the material a semi-infinite medium. For the rest of this study, it is chosen to use an insulating material and another one with a high water vapor sealing in order to ensure this first assumption. Space and time domains are defined by $\Omega_x = [\,0\,,\,L\,]$ and $\Omega_t = [\,0\,,\,t_f\,]$ respectively. $L$ represents the material dimension

along the diffusion direction. We introduce $\lambda_{ef}$ [W.m$^{-1}$.K$^{-1}$] the effective thermal conductivity and $k_m$ [s] the material total mass permeability. These two coefficients are expressed as follows :

$$k_m = k_v + k_l \,. \tag{11}$$

$$\lambda_{ef} = \lambda + h_l \, k_T \,. \tag{12}$$

Initially, temperature and vapor pressure fields are known in the material. They are positive functions defined in the spatial domain $\Omega_x = [\,0\,,\,L\,]$. In our case, material initial vapor pressure and temperature are assumed constant. The initial condition is written as follows :

$$\forall x \in [\,0\,,\,L\,], \qquad P_v\,(\,x\,,\,0\,) = P_{v0}\,, \quad T\,(\,x\,,\,0\,) = T_0\,. \tag{13}$$

Where $P_{v0}$ and $T_0$ are the material vapor pressure and temperature at the initial instant respectively. It is important to remind that these last two quantities will represent the characteristic quantities related to temperature and vapor pressure, in the dimensionless formulation part. Regarding the boundary conditions, they can be constant or vary in time. In the case of this study, the face corresponding to $x = 0$ is exposed to time-dependent heat and moisture stress. Hereafter, we consider that temperature and relative humidity at this surface are identical to those of ambient air $T^\infty$, $\phi^\infty$. This is the Dirichlet-type boundary condition, which will be the second assumption. At the exposed surface, temperature and vapor pressure are stated as follows :

$$\forall t \in [\,0\,,\,t_f\,],\, x = 0 \qquad P_v\,(\,t\,) = P_v^\infty\,(\,t\,), \quad T\,(t) = T^\infty\,(\,t\,)\,. \tag{14}$$

Furthermore, admit that the material is perfectly insulated Figure 1 and sealed against moisture on its last five faces. Thus, heat and water vapor diffusion are negligible on the other side of the material. This allows to write :

$$\forall t \in [\,0\,,\,t_f\,],\, x = L \qquad \frac{\partial P_v}{\partial x}\,(\,t\,) = 0\,, \quad \frac{\partial T}{\partial x}\,(\,t\,) = 0\,. \tag{15}$$

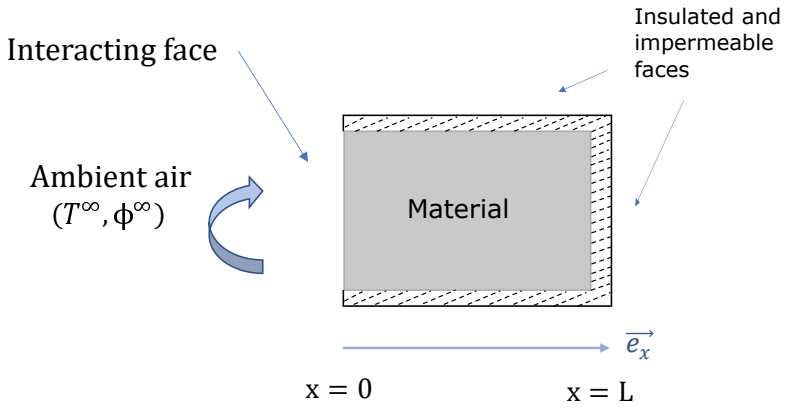


FIGURE 1 – The boundary conditions assumed in the model

In the next section, the dimensionless formulation of the problem is addressed. The aim is to obtain dimensionless equations that are independent of a given configuration. This operation is essential to obtain dimensionless numbers. These latter will be the basis for the definition of the similarity laws required for the formulated problem.

## 2.3 Dimensionless formulation

The dimensionless formulation of an equation [23, 32] requires first the definition of certain characteristic values. Afterwards, each problem variable will be reported to one of these values. For this purpose, we choose the following constants as the characteristic space and time values, $L$ the material thickness and $t_f$ experiment duration. Therefore, the first two dimensionless variables are deduced :

$$x^\star = \frac{x}{L}\,, \qquad t^\star = \frac{t}{t_f}\,. \tag{16}$$

In parallel, characteristic vapor pressure and temperature are the ones of the material at the initial state $P_{v0}$ and $T_0$. Likewise, we obtain :

$$u = \frac{P_v}{P_{v0}}\,, \qquad v = \frac{T}{T_0}\,. \tag{17}$$

Finally, all characteristic material properties are also the ones evaluated at $T = T_0$ and $P_v = P_{v0}$. Their dimensionless formulation is given as follows :

$$\rho_s^\star = \frac{\rho_s}{\rho_{s0}}\,, \quad C_m^\star = \frac{C_m}{C_{m0}}\,, \qquad k_m^\star = \frac{k_m}{k_{m0}}\,, \qquad k_T^\star = \frac{k_T}{k_{T0}}\,, \tag{18a}$$

$$\beta^\star = \frac{\beta}{\beta_0}\,, \qquad C_p^\star = \frac{C_p}{C_{p0}}\,, \qquad \lambda^\star = \frac{\lambda_{ef}}{\lambda_{ef0}}\,, \qquad \alpha^\star = \frac{\alpha}{\alpha_0}\,. \tag{18b}$$

Taking into account the scaling made on the variables of the problem, the dimensionless formulation of the equations (1) and (2) is given :

$$C_m^\star\,\rho_s^\star\,\frac{\partial u}{\partial t^\star} = \mathrm{Fo}_m\,\frac{\partial}{\partial x^\star}\left(k_m^\star\,\frac{\partial u}{\partial x^\star}\right) + \mathrm{Fo}_m\,\delta\,\frac{\partial}{\partial x^\star}\left(k_T^\star\,\frac{\partial v}{\partial x^\star}\right) + \eta\,\beta^\star\,\frac{\partial v}{\partial t^\star}\,, \tag{19}$$

$$C_p^\star\,\rho_s^\star\,\frac{\partial v}{\partial t^\star} = \mathrm{Fo}_q\,\frac{\partial}{\partial x^\star}\left(\lambda^\star\,\frac{\partial v}{\partial x^\star}\right) + \mathrm{Fo}_q\,\gamma\,\frac{\partial}{\partial x^\star}\left(\alpha^\star\,\frac{\partial u}{\partial x^\star}\right). \tag{20}$$

The dimensionless equations introduce constant and characteristic numbers [33]. First, Fourier numbers that are related to the kinetics of heat and moisture diffusion. Their expressions are given as follows :

$$\mathrm{Fo}_m = \frac{k_{m0}\,t_f}{\rho_{s0}\,C_{m0}\,L^2}\,, \qquad \mathrm{Fo}_q = \frac{\lambda_{ef0}\,t_f}{\rho_{s0}\,C_{p0}\,L^2}\,.$$

Fourier numbers represent the part of heat or moisture flux that is transmitted through the material compared to the stored heat or moisture. Differently, it is the ratio of the diffusive transport to the rate of storage. Moreover, three other characteristic numbers appear in equations (19) and (20). By definition, they describe the effect of heat or moisture diffusion on each other.

$$\delta = \frac{k_{T0}\,T_0}{k_{m0}\,P_{v0}}\,, \qquad \gamma = \frac{\alpha_0\,P_{v0}}{\lambda_{ef0}\,T_0}\,, \qquad \eta = \frac{T_0\,\beta_0}{P_{v0}\,C_{m0}\,\rho_{s0}}\,.$$

According to Equation (19), notice that the influence of heat on moisture diffusion is described by $\delta$. If $\delta < 1$, the impact of heat on moisture diffusion is minor compared to the moisture flux driven by vapor pressure. In parallel, when $\gamma < 1$, the impact of moisture on heat diffusion is minor compared to the heat driven by temperature. Finally, the number $\eta$ is a coupling

parameter for the dynamics of heat over moisture diffusion. The dimensionless formulation is applied also on the defined initial and boundary conditions. $u$ and $v$ are initially defined as follows :

$$\forall\, x^\star \in [\,0\,,\,1\,]\,, \qquad u\,(\,x^\star\,,\,0\,) = 1\,, \quad v\,(\,x^\star\,,\,0\,) = 1\,.$$

In addition, the new boundary conditions are given as follows :

$$\forall\, t^\star \in [\,0\,,\,1\,]\,,\, x^\star = L \qquad \frac{\partial u}{\partial x^\star} = 0\,, \quad \frac{\partial v}{\partial x^\star} = 0\,.$$

$$\forall\, t^\star \in [\,0\,,\,1\,]\,,\, x^\star = 0 \qquad u = u^\infty\,, \quad v = v^\infty\,.$$

After formulating the whole problem into a dimensionless form, we reach a configuration, where the quantities $u$ and $v$ do not depend anymore on the parameters of the physical model. Only the characteristic numbers are used to evaluate the variation of these fields. Consequently, the concept of similarity laws is introduced. The following section will thus consist in defining these laws and presenting their applications in fields of applied physics.

## 2.4 Similarity laws on heat and moisture diffusion

In order to apply these laws, two different configurations indexed by 1 and 2 are introduced. The first configuration is defined by the space domain $\Omega_x^1 = [\,0\,,\,L_1\,]$ and time domain $\Omega_t^1 = [\,0\,,\,t_{f\,1}\,]$. The same for the second one where $\Omega_x^2 = [\,0\,,\,L_2\,]$ and $\Omega_t^2 = [\,0\,,\,t_{f\,2}\,]$. Where $L_1$ and $L_2$ represent the thicknesses of the material in configuration 1 and 2 respectively. Likewise for $t_f$ which represents the duration of an experiment. Based on the latter, two configurations are stated similar if the dimensionless formulation of the problem is identical in both cases. This implies that the dimensionless numbers are equal in both configurations. Thus, it is deduced from Eqs. (19) and (20) the following :

$$\mathrm{Fo}_{m\,1} = \mathrm{Fo}_{m\,2}\,, \qquad \mathrm{Fo}_{q\,1} = \mathrm{Fo}_{q\,2}\,, \tag{21a}$$

$$\delta_1 = \delta_2\,, \qquad \gamma_1 = \gamma_2\,, \qquad \eta_1 = \eta_2\,. \tag{21b}$$

In our study, the cases consist of two samples representing the same material and initially conditioned at the same temperature and vapor pressure. This implies that :

$$T_{0\,1} = T_{0\,2}\,, \qquad P_{v\,0\,1} = P_{v\,0\,2}\,.$$

Not changing the material from one configuration to another helps setting the assumption 4. Thus, notice that the equality on numbers $\delta$, $\gamma$ et $\eta$ in Equation 21b is guaranteed . Moreover, the equivalence on heat and moisture Fourier numbers enables to obtain :

$$\frac{t_{f\,1}}{L_1^2} = \frac{t_{f\,2}}{L_2^2}\,. \tag{22}$$

Recalling that the properties $\rho_{s\,0}$, $k_{m\,0}$, $C_{m\,0}$, $\lambda_0$ and $C_{p\,0}$ are considered equal in both configurations.

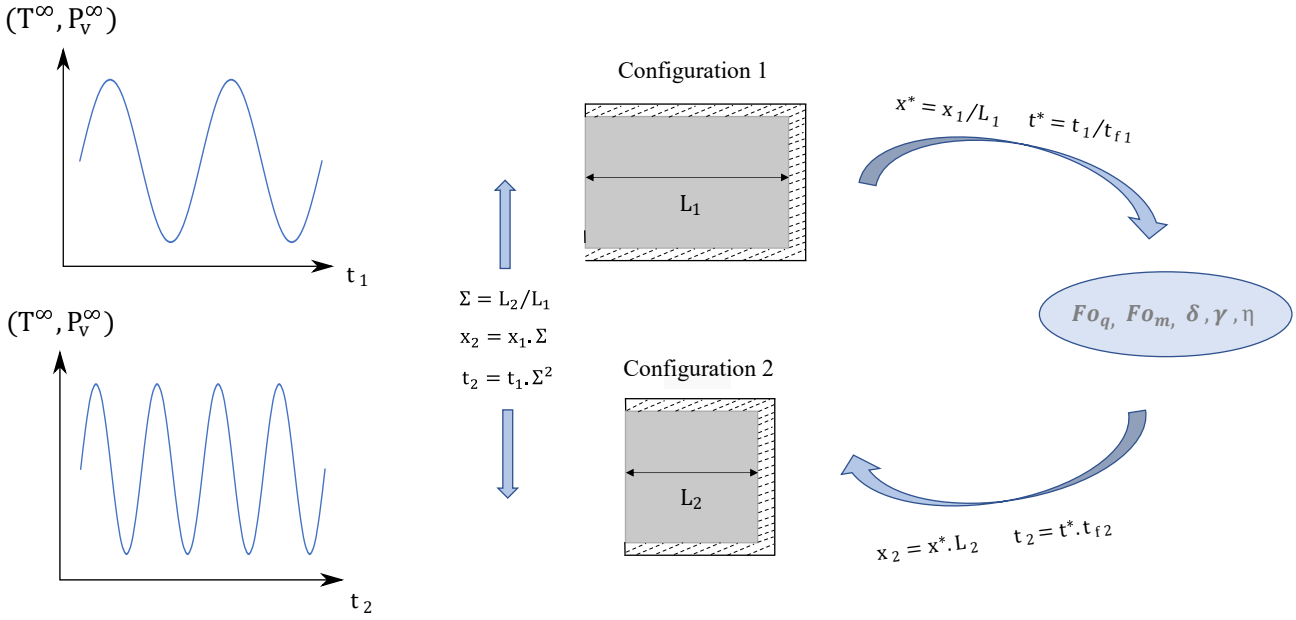


FIGURE 2 – The mapping between two configurations 1 and 2

Remark that similarities create space-time equivalences between configurations. In this regard, the similarity proportionality factor $\Sigma$ is defined which is a length ratio and defined as follows :

$$\Sigma = \frac{L_2}{L_1}\,. \tag{23}$$

When $\Sigma < 1$, *i.e.* $L_2 < L_1$, the space dimension of the reference configuration is reduced. This possibility constitutes our choice in order to overcome the slow kinetics of heat and moisture diffusion. Therefore, our objective would be to deal with a long experimental configuration called reference while working on a reduced design. Given that the duration of the long and short experiments are $t_1$ and $t_2$ respectively, an equivalence is set between these experiments if they verify :

$$t_{f\,2} = t_{f\,1}\,\Sigma^2\,. \tag{24}$$

In reality, assumption 3 is true only if the micro-structure of a sample remains unchanged going from the reference configuration to the reduced model. Ideally, the properties and their laws of variation are identical if it is assumed that the reduced configuration represents a sample that is identical to the one in the reference configuration in terms of porosity, tortuosity and pore size distribution. Note that the time scale of the reduced configuration is modified by two orders compared to the space scale. From a mathematical perspective, a mapping is carried Figure 2 linking the reference configuration to the equivalent one by means of the proportionality factor (23). This mapping is ensured through the obtained dimensionless numbers. Thus, it is formulated in the following way :

$$\Omega_x^1 \times \Omega_t^1 \longmapsto \Omega_x^2 \times \Omega_t^2\,,$$

$$\left(x_1\,,\,t_1\right) \longmapsto \left(x_2 = x_1 \cdot \Sigma\,,\,t_2 = t_1 \cdot \Sigma^2\right).$$

## 2.5 Experimental assessment of the validity of similarity law

After defining the equivalent configurations 1 and 2, the experimental validation of the similarity laws is carried out by comparing temperature and relative humidity in both configurations. Indeed, the equivalence in temperature and vapor pressure induces that of relative humidity. This comparison can be carried according to the physical domain. In this case, for $x_1 \in \Omega_x^1$, $x_2 \in \Omega_x^2$, $t_1 \in \Omega_t^1$ and $t_2 \in \Omega_t^2$ such that $x_2 = x_1\,\Sigma$ and $t_2 = t_1\,\Sigma^2$, the following affirmations must be verified :

$$T(x_1, t_1) = T(x_2, t_2) \quad , \quad \phi(x_1, t_1) = \phi(x_2, t_2)\,. \tag{25}$$

Where $\phi$ represents the relative humidity that is defined according to Eq. (26) :

$$\phi = \frac{P_v}{P_{sat}}\,. \tag{26}$$

To validate the laws of similarity on this problem, discrepancies and total uncertainties should be estimated and compared. In this regard, the results related to the reference and reduced configurations are in agreement if :

$$\left|\epsilon_T(\chi_i, t)\right| \leq \sigma_T(\chi_i, t) + \sigma_T(\chi_i\,\Sigma, t\,\Sigma^2)\,, \tag{27a}$$

$$\left|\epsilon_\phi(\chi_i, t)\right| \leq \sigma_\phi(\chi_i, t) + \sigma_\phi(\chi_i\,\Sigma, t\,\Sigma^2)\,. \tag{27b}$$

Where $\chi_i \in [0, L_i]$ is a position within the material in the reference configuration considering that $i \in \{1, 2\}$ and $t \in [0, t_{fi}]$ are the instants during this same configuration. According to Eqs. (27a) and (27b), It should be ensured that the discrepancy one a given field ($\epsilon_\phi$ or $\epsilon_T$) as expressed in Equations (28a) and (28b), between two similar positions and at equivalent instants, is smaller in absolute value than the sum of the total uncertainties ($\sigma_T$, $\sigma_\phi$). In the following section, the manufacturing phase of the material is evidenced. It is resumed to the formulation of samples, the used molds and the necessary curing period. Subsequently, the necessary devices and equipment are exposed. Finally, the samples which represent the reference and reduced configurations will also be announced.

$$\epsilon_T(\chi_i, t) = T(\chi_i, t) - T(\chi_i\,\Sigma, t\,\Sigma^2)\,, \tag{28a}$$

$$\epsilon_\phi(\chi_i, t) = \phi(\chi_i, t) - \phi(\chi_i\,\Sigma, t\,\Sigma^2) \tag{28b}$$

# 3 Experimental investigation

## 3.1 Material

FIGURE 3 – Formulation of the $15 \times 15 \times 15\,\mathsf{cm}^3$ samples

The tests, presented in this work, are performed on hemp concrete samples. It is a bio-based material with the substitution of hemp plant fibers [34]. All samples are derived from the same formulation. The manufacture of this material was described thanks to the standardization according to NF EN 459, NFP $15-314$ and NF EN $197-1$. It imposes the following mass fractions : 16% of hemp, 34% of cement and 50% of water.

The hemp is issued from the Biofibat product. It is an aggregate made up exclusively of cellulose fibers, calibrated and dust-free, resulting from the defibration of hemp straw. The product technical description shows the following values : $\rho = 110\,\mathsf{kg.m}^{-3}$, $\lambda = 0.05\,\mathsf{W.m}^{-1}.\mathsf{K}^{-1}$. These properties were evaluated at 15% moisture content. Tradical$^{\mathrm{R}}$ PF70 is a formulated lime of class FL A 3.5, valid according to the NF 459 standard. This lime is designed to produce mortars for natural stone, hollow or full bricks, as well as traditional plasters. According to the manufacturer, the lime is characterized at the dry state as follows : $\rho_s = 620\,\mathsf{kg.m}^{-3}$, $\lambda_s = 0.2\,\mathsf{W.m}^{-1}.\mathsf{K}^{-1}$.

In an industrial container, the correct proportions of water and lime are mixed for three minutes via a double speed mixer. A good hydration is ensured by the sufficient appearance of water bubbles. Then, hemp is added to the container and mixed for another 2 minutes. Afterwards, the obtained mixture is filled into $15 \times 15 \times 15\,\mathsf{cm}^3$ molds. These are treated with a specific oil in order to facilitate the releasing. After ten days of hydration, the samples are obtained and stored in ambient air conditions for three months. The experimental characterization of heat and moisture properties of hemp concrete provided the following results at the dry state : $\lambda_s = 100.23\,\mathsf{mW.m}^{-1}.\mathsf{K}^{-1}$, $C_{ps} = 1150\,\mathsf{J.kg}^{-1}.\mathsf{K}^{-1}$, $\rho_s = 480\,\mathsf{kg.m}^3$, $k_v = 2.8\,10^{-11}\,\mathsf{s}$ and $k_l = 7.4\,10^{-13}\,\mathsf{s}$.

$$\omega = \frac{m\,K\,\phi}{1+K\,\phi}\,\frac{1-k\,(1-w)}{1-k\,\phi}\,. \tag{29}$$

For the determination of the average sorption curve of hemp concrete, the experimental

results in [35] are used. The data are obtained for the same formulation of hemp concrete, at $T = 25\,°\mathsf{C}$ and for different relative humidity values. Subsequently, the experimental curve was fitted using the Generalised D′arcy and Watt model (GDW) for the sorption curves which is given according to Eq. (29). Based on the performed fitting, the parameters of this model are estimated as : $m = 0.068$, $K = 2.722$, $k = 0.964$ and $w = 0.187$.

## 3.2 Experimental equipment


FIGURE 4 – The climatic chamber used in tests

After the hydration of the samples, they are put under different experimental tests. It consists mainly in generating realistic climate conditions to apply on samples. This task was carried out thanks to a climatic chamber of CTS mark illustrated in the Figure 4. It is a cell having the dimensions $0.9 \times 1 \times 1.6\,\mathsf{m}^3$, ensuring a use range from $-70$ to $180\,°\mathsf{C}$ in temperature and 10 to 98% in relative humidity. During the material exposure, temperature and relative humidity are measured at different locations using capacity humidity sensors. These are manufactured by Ahlborn, and have a diameter of $5\,\mathsf{mm}$ (Figure 5a). The operating ranges for temperature and relative humidity are $-30$ to $100\,°\mathsf{C}$ and 5 to 98% respectively. Furthermore, based on the factory calibration certificate, the systematic accuracy of these sensors are given as $\sigma_{T,Sys} = 0.3\,°\mathsf{C}$ and $\sigma_{\phi,Sys} = 4\%$ for temperature and relative humidity respectively. These values are obtained at a nominal temperature of $25\,°\mathsf{C}$. During experiments, assume that the systematic accuracy do not depend on either measurement position or instant according to assumption 6. Indeed, the sensors are calibrated in relative humidity for values lower than 90% and at a temperature of $25\,°\mathsf{C}$. Thus, 4% uncertainty in relative humidity is assumed. In temperature, three systematic uncertainties are provided for three different ranges of variation. The chosen uncertainty in temperature is given for a range from 0 to $70\,°\mathsf{C}$. Based on these data, the considered systematic uncertainties are fully justified for temperature and relative humidity variations in this study. The response time of the sensor is around $10\,\mathsf{s}$ for a maximum of $1\,\mathsf{m.s}^{-1}$ air flow velocity. The display and recording of data each is ensured $5\,\mathsf{min}$ by the use of an acquisition unit and a memory card of Almemo brand shown in Figure 5b. The choice to record results on a minute-scale can be justified. The link can be made with the kinetics of

heat and moisture diffusion. It was agreed that the recording should be on this scale because of a compromise between both transfer natures. Indeed, heat transfer is a purely diffusive phenomenon and is relatively faster than moisture transfer. The latter, requiring available open pore networks, represents a transport phenomenon. A recording on an hour-scale, for example, would be suitable to measure only relative humidity. However, since sensors measure simultaneously temperature and relative humidity, it is rather decided to take into account first the quick variation in temperature. Consequently, the interval between each measurement is set shorter, on a minute-scale.

The described equipment will initially be used to test the hypotheses in Section 2.2. Assumption 1 will not be assessed in this study. Indeed, it is assumed verified on the basis of the work in [22], where it was dealt with a heat diffusion investigation. In the latter, a hemp concrete sample, insulated and sealed in the same way as in the two configurations, was exposed to variable heat stress. The one-dimensional transfer assumption was assessed following two different approaches. A first experimental investigation was carried out where the flux along the $x$-axis (transfer direction) is compared to the one along the $y$-axis. These fluxes are calculated using finite differences with a centered scheme and sensors around the chosen position where $\Delta x = \Delta y = 5\,\mathsf{cm}$. It was shown that the flux along $y$ represents 5 to 9% of the one along the privileged direction. In the same work, a second approach consisted in investigating numerically the same fluxes by simulating the thermal behavior of hemp concrete. This time, the resolution method was based on finite elements where $\Delta x = \Delta y = 10^{-3}\,\mathsf{cm}$. Results showed that the flux along $y$ does not exceed 1% of the one along $x$. Note that both approaches confirm the validity of this assumption within a certain error. The latter is more important in the experimental investigation because of the large mesh size. This could not be refined due to constraints related to the experimental design. The following part will be dedicated to the description of the experimental procedure aiming to evaluate the Assumption 2.


(a) Ahlborn sensors


(b) Display screen

## 3.3 Experimental procedure to evaluate the assumption 2 on the Dirichlet condition modeling

In assumption 2, it is assumed that air temperature and vapor pressure are the ones at the exposed material surface. However, this statement defines Dirichlet boundary conditions.

Indeed, the latter requires in this case the knowledge of temperature and vapor pressure at the surface of the material. In reality, a heat and moisture resistance exist and which define the interaction between a material and air. In this case, these interactions at the interface are defined thanks to the condition of Robin, whose dimensionless formulation induces the Biot number. Its expression for both heat and moisture diffusion is given as follows :

$$\mathrm{Bi_q} = \frac{h_c\, L}{\lambda}\,, \qquad \mathrm{Bi_m} = \frac{h_m\, L}{k_m}\,. \tag{30}$$

Where $h_c\,[\mathsf{W.m^{-2}.K^{-1}}]$ and $h_m\,[\mathsf{kg.m^{-2}.s^{-1}.Pa^{-1}}]$ are the surface heat and moisture diffusion coefficients respectively. In this field, Biot numbers designate the ratio of heat or moisture diffusion resistance at the surface and inside the material. When $\mathrm{Bi}_{q,m} > 1$, the diffusion inside the material is slower than the heat or moisture reaching the exposed surface. According to the preceding, the second assumption is more justified if the Biot number is large. This implies a great surface diffusion coefficient. Moreover, most empirical laws, expressing this coefficient, link it directly to air velocity [36, 37]. Thus, it follows that assumption 2 is more reliable if tests are performed using high air flow velocity ranges. Concerning this test, the first step is selecting a sample which is $L = 10\,\mathsf{cm}$ thick and exposing it to the conditions presented in the mathematical model in Section 2.2. Note that the sample undergoes a preliminary preconditioning step where air temperature and relative humidity are set at $T = 23\,^{\circ}\mathsf{C}$ and $\phi = 50\,\%$ respectively. Additionally, it is necessary to ensure that heat and moisture diffusion are one-dimensional. In order to validate this condition, we use a $5\,\mathsf{cm}$ thick layer of synthetic thermal insulator made of polyethylene. For a good moisture sealing, an additional layer of a low-permeability aluminum band is employed. In addition, the surface defined by the equation $x = L$ is insulated in the same way. Indeed, heat and moisture flux must be negligible at $x = L$.

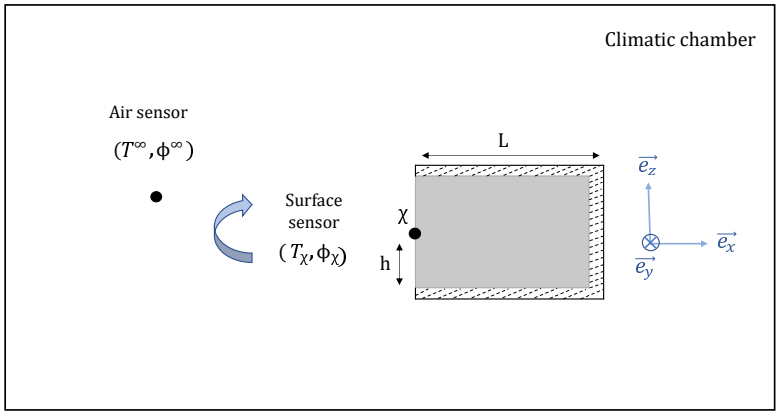


FIGURE 6 – Illustration of the experimental configuration to assess the validity of assumption 2 (Dirichlet boundary condition)

The second step consists in using two Ahlborn sensors as shown in Figure 6. The first one is positioned on the node $\chi\,(\,x = 0\,,\, y = l\,,\, z = h\,)$ where $l = h = 5\,\mathsf{cm}$. It can be fixed using an adhesive ribbon, while the second is suspended inside the climatic chamber. Afterwards, the sample is put in the cell while creating the climatic stress scenario.

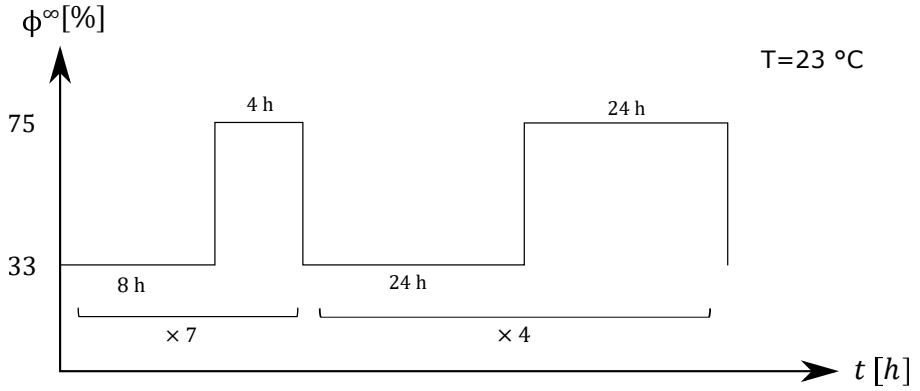


FIGURE 7 – Hydric stress considered for the verification test of the assumption 2

Throughout the experiment, the same temperature during the preconditioning is maintained. Moreover, air relative humidity varies between two values 33 % and 75 % as shown in Figure 7. According to the latter, the presence of two phases is observed, a drying at 33 % then humidification at 75 %. Additionally, the experiment duration is split into two parts. During the first one, the sample undergoes 7 cycles. Each cycle consists of setting 33 % relative humidity for 8 hours, then 75 % for 4 hours. As for the second part, it is longer and consists of only 4 cycles. These latter include drying during 24 hours and humidification considering the same duration. The goal is to follow the variation in temperature as well as the relative humidity of both sensor positions. Thus, errors $\varepsilon_{T_s}$ and $\varepsilon_{\phi_s}$ are deduced with regard to the assumption 2.

$$\varepsilon_{T_s}(t) = \left| T(\chi, t) - T^{\infty}(t) \right|, \qquad \varepsilon_{\phi_s}(t) = \left| \phi(\chi, t) - \phi^{\infty}(t) \right|. \tag{31}$$

The evaluation of both errors is essential to discuss the limits of this assumption. In this context, both errors are compared in terms of magnitude. In particular, these data are necessary for the evaluation of the uncertainties [38] related to this assumption. After describing the experimental procedure, the next part defines the tests which aim to verify, under the defined hypotheses, the law of similarities.

## 3.4 Experimental procedure to assess the heat and mass similarity

Three months after the material formulation, two samples are selected to assess the validity of similarity. The goal is to create two equivalent configurations in regard to these laws. The configurations 1 and 2 are denoted reference and reduced, respectively. In this case, $\Sigma < 1$ ($L_{ref} > L_{red}$), which means a reduction of time and space scales of the reference configuration. For this purpose, a one sample is sliced to ensure the desired thickness. Then, both samples undergo the same preconditioning phase for 15 days under a temperature of 23 °C and a relative humidity of 50%. Afterwards, both samples are insulated and sealed as explained in Section 3.3. In each configuration, two sensors are placed at two different sample depths. In order to compare the experimental results between both configurations, the positions chosen must verify the following condition :

$$\chi_{red} = \chi_{ref}\, \Sigma\,.$$

Regarding the boundary conditions, a dynamic stress scenario is considered for the reference configuration with a duration $t_{ref}$. In this case, similarity imposes the adoption of the same scenario in terms of magnitude, but reduced in duration. In particular, the duration of the reduced test must satisfy this equality :

$$t_{red} = \Sigma^2 \, t_{ref} \, .$$

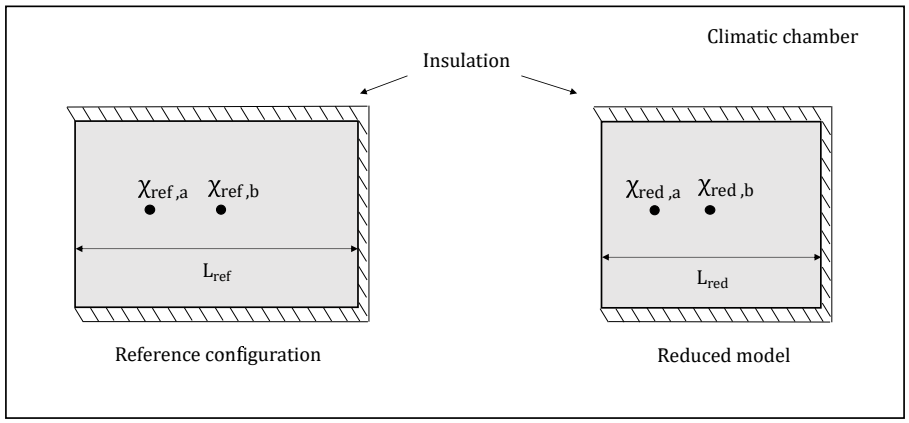


FIGURE 8 – The similar experimental configurations

The chosen set of positions to carry a comparison is the quarter and middle of the sample. According to the Figure 8, an experimental confrontation is performed in temperature and relative humidity between $\chi_{ref,a}$ and $\chi_{red,a}$ as well as between $\chi_{ref,b}$ and $\chi_{red,b}$.

## 3.5 Definition of the study case

In order to apply similarities, a first configuration is considered and designated reference. It is based on a hemp concrete sample where $L_{ref} = 10\,[\mathsf{cm}]$. First, temperature and relative humidity were set at $T_0 = 23\,[^\circ\mathsf{C}]$ and $\phi_0 = 50\,[\%]$. Afterwards, boundary conditions are defined by an air relative humidity which varies as shown in Figure 7 where temperature remains constant and equals $T^\infty = 23\,[^\circ\mathsf{C}]$. Moreover, the experiment duration is set to $t_{ref} = 11.5\,[\mathsf{d}]$. In order to compare temperature and relative humidity between configurations, two sensors were positioned at the positions whose coordinates are : $\chi_{ref\,a} = 2.5\,[\mathsf{cm}]$ and $\chi_{ref\,b} = 5\,[\mathsf{cm}]$ along the $x$ axis.

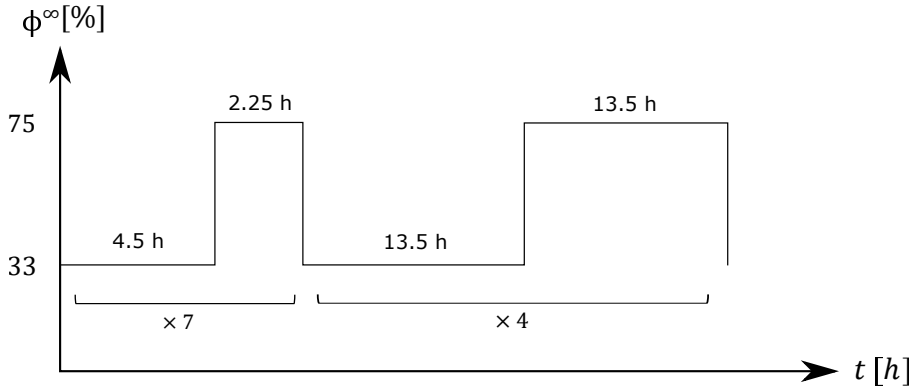


FIGURE 9 – Moisture stress applied in the reduced configuration

Hereafter, the factor proportionality is set to $\Sigma = 0.75\,[-]$ to deduce the second equivalent configuration which is denoted reduced. Relying on this, the reference sample underwent a 25 % scale reduction along the $x$ axis. Thus, the reduced thickness is obtained $L_{red} = \Sigma\, L_{ref} = 7.5\,[\mathsf{cm}]$. Additionally, similarity requires the same preconditioning for the reduced sample in temperature and relative humidity. As for the boundary conditions, the duration is reduced in the equivalent configuration. According to Eq. (24), the periodicity of the experiment is decreased by 43.75 %. Indeed, the reduced sample should undergo a stress which lasts $t_{red} = \Sigma^2\, t_{ref} = 6.47\,[\mathsf{d}]$. The reduced stress scenario is shown in Figure 9. Finally, the equivalent positions inside the reduced sample are obtained by applying the proportionality factor on $\chi_{ref,a}$ and $\chi_{ref,b}$. Therefore, $\chi_{red,a} = \Sigma\, \chi_{ref,a} = 1.875\,[\mathsf{cm}]$ and $\chi_{red,b} = \Sigma\, \chi_{ref,b} = 3.75\,[\mathsf{cm}]$. Remind that this four positions have the same coordinates along $y$ and $z$ axis.

In section 4, the notion of uncertainties is discussed. In the first place, a definition and the utility of this quantity are given. Then, in the framework of our study, the global uncertainty is formulated. With further details, different sub-uncertainties are identified by defining and expressing them analytically.

# 4 Evaluation of uncertainties related to heat and moisture diffusion experiment

During any experiment, there are certain sources of error that are unavoidable and that influence a result. These can include the calibration, environmental conditions during the experiment, manipulator behavior or even the response time of a used device. Thus, it is important for the experimenter to be able to define the margin of error related to his measurements. As similarity experiments are exposed to sources of errors, both tests are associated to two global uncertainties $\sigma_T$ and $\sigma_\phi\,[^\circ\mathsf{C}]$. According to Taylor [39, 40], uncertainties on temperature and relative humidity are expressed as follows :

$$\sigma_T^2 = \sigma_{T,\mathrm{Sys}}^2 + \sigma_{T,x}^2 + \sigma_{T,t}^2 + \sigma_{T,\mathrm{Rdm}}^2 + \sigma_{T,\mathrm{H2}}^2\,. \tag{32a}$$

$$\sigma_\phi^2 = \sigma_{\phi,\mathrm{Sys}}^2 + \sigma_{\phi,x}^2 + \sigma_{\phi,t}^2 + \sigma_{\phi,\mathrm{Rdm}}^2 + \sigma_{\phi,\mathrm{H2}}^2\,. \tag{32b}$$

$\sigma_T$ and $\sigma_\phi$ are the global uncertainties associated to temperature and relative humidity fields respectively. According to Equations (32a) and (32b), it was chosen to limit at five the number of sub-uncertainties. The assessment of a global uncertainty helps defining the confidence interval related to an experimental result. Mathematically, confidence intervals related to temperature or relative humidity and denoted $I_T$ and $I_\phi$, respectively, are defined as follows :

$$I_T(\chi, t) = \left\{ m \in \mathbb{R}^+; \quad T(\chi, t) - \sigma_T(\chi, t) \leq m \leq T(\chi, t) + \sigma_T(\chi, t) \right\}, \tag{33a}$$

$$I_\phi(\chi, t) = \left\{ m \in \mathbb{R}^+; \quad \phi(\chi, t) - \sigma_\phi(\chi, t) \leq m \leq \phi(\chi, t) + \sigma_\phi(\chi, t) \right\}. \tag{33b}$$

Where $\chi$ and $t$ define the measurement position and the instant of the experiment, respectively.

## 4.1 Systematic uncertainty

Starting with $\sigma_{T,\,\mathrm{Sys}}$ and $\sigma_{\phi,\,\mathrm{Sys}}\,[°\mathsf{C}]$, which are the systematic uncertainties on both fields and related to the sensors used for the measurements. They arise from the sensor calibration defects and are provided by the manufacturer [41]. Moreover, they depend on the temperature and relative humidity ranges that a sensor measures. In this study, it is assumed that this uncertainty is constant during carried experiments. Their values are given in Section 3.2.

## 4.2 Uncertainty related to sensor position

Another source of error could result from the sensor position accuracy. It is taken into account since the experimenter runs the risk of being inaccurate, and also because of the diameter of used sensors. In this purpose, the uncertainties $\sigma_{T,x}$ and $\sigma_{\phi,x}\,[°\mathsf{C}]$ regarding the sensor position are expressed as follows :

$$\sigma_{T,x}(x, t) = \frac{\partial T}{\partial x}\,\delta_x + o(\delta_x), \tag{34a}$$

$$\sigma_{\phi,x}(x, t) = \frac{\partial \phi}{\partial x}\,\delta_x + o(\delta_x). \tag{34b}$$

Where :

$$\frac{\partial \phi}{\partial x} = \frac{1}{P_{sat}}\frac{\partial P_v}{\partial x} - \frac{P_v}{P_{sat}^2}\frac{\partial P_{sat}}{\partial T}\frac{\partial T}{\partial x}. \tag{35}$$

The saturation pressure derivative according to temperature is given by the relation of Clapeyron in Eq. (36) :

$$\frac{\partial P_{sat}}{\partial T} = \frac{M\,L_v}{R\,T^2}\,P_{sat}. \tag{36}$$

As for this uncertainty, it depends on time and space. It is based on the infinitesimal development of temperature and relative humidity around the sensor position. Particularly, this development is limited to the first order. The partial derivatives are evaluated, at the desired location and instant, by solving Eqs. (1) and (2). For that, finite elements method is used. In addition, $\delta_x\,[\mathsf{m}]$ designates the distance that represents the error committed on the position of the sensor. This error is mainly due to the drilling of a material and introducing the sensors. The order of magnitude of $\delta_x$ is assumed equivalent to the diameter of the sensor.

## 4.3 Uncertainty related to sensor response time

The response time of a sensor can also impact an experimental result. It describes the reaction of a sensor following a change in temperature or relative humidity. The less time a sensor takes to display the correct value, the more accurate it is. Thus, the sensor time response uncertainty is defined by :

$$\sigma_{T,t}\,(\,x\,,\,t\,) = \frac{\partial T}{\partial t}\,\delta_t + o\,(\,\delta_t\,)\,. \tag{37a}$$

$$\sigma_{\phi,t}\,(\,x\,,\,t\,) = \frac{\partial \phi}{\partial t}\,\delta_t + o\,(\,\delta_t\,)\,. \tag{37b}$$

Where :

$$\frac{\partial \phi}{\partial t} = \frac{1}{P_{sat}}\,\frac{\partial P_v}{\partial t} - \frac{P_v}{P_{sat}^2}\,\frac{\partial P_{sat}}{\partial T}\,\frac{\partial T}{\partial t}\,. \tag{38}$$

$\sigma_{T,t}$ and $\sigma_{\phi,t}\,[°\mathsf{C}]$ vary also according to time and space. The temporal partial derivatives are determined, in the same way, based on the solution computation of Eqs. (**??**) and (**??**). $\delta_t\,[\mathsf{s}]$ represents the response time of the sensor. Its value for Ahlborn sensors is given in Section 3.2.

## 4.4 Random uncertainty

Equations (32a) and (32b) introduce each a fourth term which is $\sigma_{T,\,\mathrm{Rdm}}$ or $\sigma_{\phi,\,\mathrm{Rdm}}\,[°\mathsf{C}]$. This uncertainty characterizes the random aspect of a given experiment. Generally, it constitutes the parameter which is used to evaluate the reproducibility of a test. Particularly, it informs on the variability of the micro-structure from one sample to another. Consider N samples undergoing the same experiment. And let $T_i$ and $\phi_i$ be the temperature and relative humidity measured in the sample $i$ at the instant $t$ where $i \in \{\,1\,,\,N\,\}$. $\bar{T}$ and $\bar{\phi}$ are the arithmetic means of both fields respectively for N samples. The random uncertainty is given by the formula below :

$$\sigma_{T,\,\mathrm{Rdm}}\,(\,x\,,\,t\,) = \frac{1}{N^{\,1/2}}\left(\,\frac{1}{N-1}\,\sum_{i=1}^{N}\,(\,T_i - \bar{T}\,)^{\,2}\,\right)^{1/2}, \qquad \bar{T} = \frac{1}{N}\,\sum_{i=1}^{N}\,T_i\,. \tag{39a}$$

$$\sigma_{\phi,\,\mathrm{Rdm}}\,(\,x\,,\,t\,) = \frac{1}{N^{\,1/2}}\left(\,\frac{1}{N-1}\,\sum_{i=1}^{N}\,(\,\phi_i - \bar{\phi}\,)^{\,2}\,\right)^{1/2}, \qquad \bar{\phi} = \frac{1}{N}\,\sum_{i=1}^{N}\,\phi_i\,. \tag{39b}$$

Note that the random uncertainty is a time function because temperature and relative humidity and their averages are as well. Moreover, these parameters are evaluated at positions where the study is carried.

## 4.5 Assumption 2 uncertainty

Finally, this uncertainty involves the evaluation of the error related to the modeling of the Dirichlet type boundary condition. On the one hand, it is based on the study of the sensitivity on temperature and relative humidity within the material in regard to those at the interaction surface. On the other hand, it depends on the discrepancy in a field between the interaction surface and air. $\sigma_{T,\,\mathrm{H2}}$ and $\sigma_{\phi,\,\mathrm{H2}}$ are expressed via the Eqs. (40a) and (40b) :

$$\sigma_{T,\,\mathrm{H2}}\,(\,x\,,\,t\,) = \frac{\partial T}{\partial T_s}\,\delta_{T_s} + o\,(\,\delta_{T_s}\,)\,, \tag{40a}$$

$$\sigma_{\phi,\mathrm{H2}}(x,t) = \frac{\partial \phi}{\partial \phi_s}\,\delta_{\phi_s} + o(\delta_{T_s}). \tag{40b}$$

Where $T_s$ and $\phi_s$ are the temperature and relative humidity at the interaction surface respectively. Furthermore, $\delta_{Ts}$ and $\delta_{\phi s}$ represent the discrepancy in temperature and relative humidity between air and the material surface. These two quantities are evaluated experimentally thanks to the used sensors. Concerning the partial derivatives, they are calculated numerically by carrying out a study of sensitivity according to surface temperature and relative humidity. Furthermore, these derivatives are denoted $\theta_1$ and $\theta_2$ such that :

$$\theta_1 = \frac{\partial T}{\partial T_s}, \qquad \theta_3 = \frac{\partial \phi}{\partial \phi_s}. \tag{41}$$

In the section 1 of the appendix, the governing equation related to both quantities $\theta_1$ and $\theta_2$ are detailed.

# 5 Results and discussion

## 5.1 Experimental evaluation of the assumption : Dirichlet condition modeling

The objective is to evaluate temperature and relative humidity discrepancies $\delta_{T_s}$ and $\delta_{\phi_s}$, introduced in Eq. (31), between the material surface and the air inside the chamber.

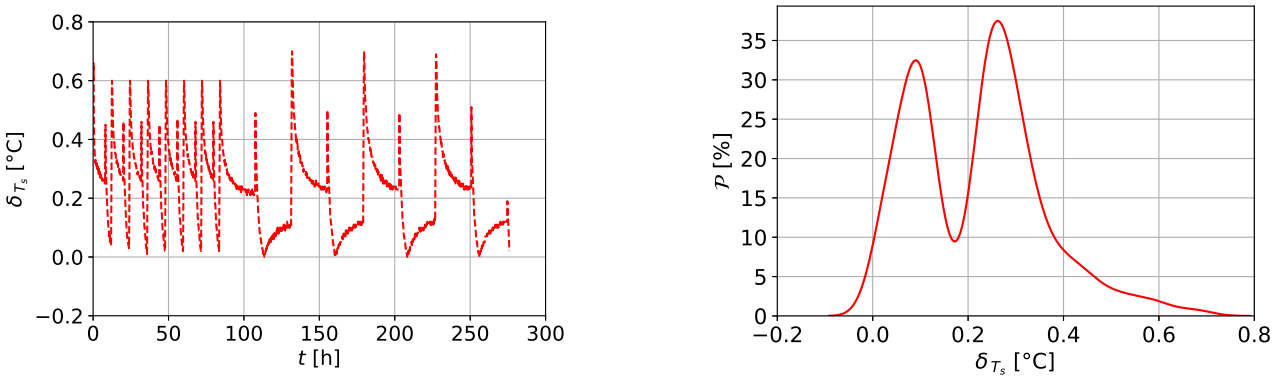


(a) (b)

FIGURE 10 – (a) Temperature discrepancy between air and the sample surface, (b) Probability density related to the discrepancy on temperature

Despite maintaining a constant temperature, periodic fluctuations are noticed Figure 10a. This can be explained by the impact of moisture diffusion on the temperature variation. In addition, this latter follows the periodicity of the moisture stress. Furthermore, the variation in $\delta_{T_s}$ follows two different periodicity which are the same as the ones defining the experiment cycles. During the first 7 cycles, $\delta_{T_s}$ varies from 0 to 0.6 °C. As for the following cycles, the curve remains almost in the same shape but has larger periodicity. In this case, $\delta_{T_s}$ reaches maximum values slightly higher 0.7 °C than those during the first cycles. Moreover, Figure 10b highlights

the variation of a new function which will be used frequently in next Sections. It is the probability density and denoted $\mathcal{P}$ [42, 43]. It calculates $\delta_{T_s}$ values distribution. In this work, the Kernel distribution is adopted as a probability density. It is based on the Parzen – Rosenblatt method. The latter helps to estimate the density at each point of an interval. Contrary to other methods, namely the one introduced by Rudemo or Bowman, it is more accurate. This method generalizes the histogram estimation method which is not continuous. For this, the bar centered at a given value and considering a smoothing parameter, is replaced by a Gaussian centered at this same value. By analyzing the curve in Figure 10b, $\mathcal{P}$ represent two local maximums. First one around 0.1 °C with a probability of 32 %. Then, we reach another maximum of 37 % around 0.25 °C.

In terms of relative humidity, $\delta_{\phi_s}$ is plotted in Figure 11a. Similarly to temperature, the discrepancy on relative humidity varies in accordance with two periodicity. During short cycles, $\delta_{\phi_s}$ varies between 0 and 0.062. As for long cycles, the discrepancy is relatively smaller. Indeed, it ranges this time between 0 and 0.054. Moreover, large discrepancies are due to transitions from 0.33 to 0.75 and vice versa. Notice also that discrepancy reaches 0 many times during the second phase. The reason behind is the cycle duration in the experiment second part, which is longer.

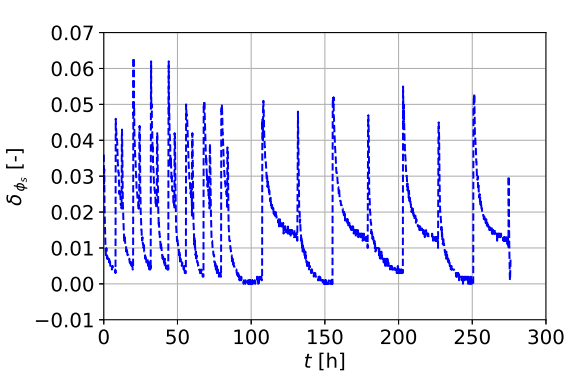


(a)

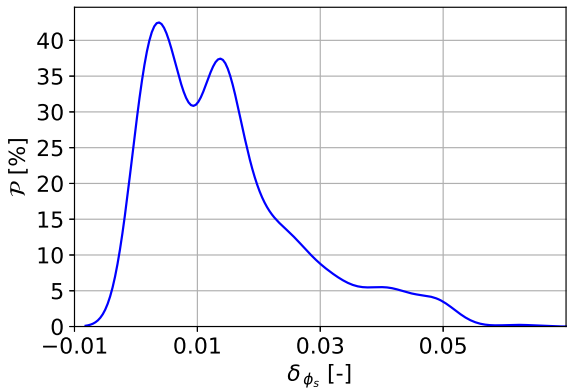


(b)

FIGURE 11 – (a) Discrepancy on relative humidity between air and the sample surface, (b) Probability density representing this discrepancy

Indeed, maintaining a constant air relative humidity for longer helps decreasing the discrepancy between $\phi^{\infty}$ and $\phi_s$. Focusing on the distribution of values taken by $\delta_{\phi_s}$, it is assessed and illustrated according to Figure 11b. Based on that, probability density takes maximum values ranging from 30 % to 40 % for discrepancies between 0 and 0.02 approximately. In addition, notice that zero discrepancy is reached with about 27 % of probability. Hence, based on the results of temperature and relative humidity errors, it is deduced that the assumption 2 is not quite ensured. To conclude, the discrepancy in temperature is different from 0 in 90 % of the experiment instants. However, the order of magnitude is not very significant. On the other hand, $\delta_{\phi_s}$ turns to 0 in 27 % of the cases, thus a small improvement is observed when comparing the results of these two discrepancies. Nevertheless, the values reached by $\delta_{\phi_s}$ are more meaningful, going up to 0.06. In this case, this would have a consequent effect on the similarities study especially in terms of relative humidity. Regarding this fact, it is decided to

include these data in the uncertainty investigation.

In the next Sub-section, the necessary conditions are first recalled to create a similarity between two different configurations. Subsequently, these latter are introduced with their physical dimensions and boundary conditions.

## 5.2 Assessment of heat and moisture diffusion similarity

This Section deals with the evaluation of uncertainties on temperature and relative humidity in both configurations. It includes a first part where numerical schemes and an experimental methodology are presented. Subsequently, the variation of each sub-uncertainty is analyzed and compared between both configurations. To facilitate comparison, the colors blue and red are used to represent the reference and reduced configurations, respectively. Finally, temperature and relative similarity is assessed and discussed.

### 5.2.1 Assessment of the uncertainty in reference and reduced configuration

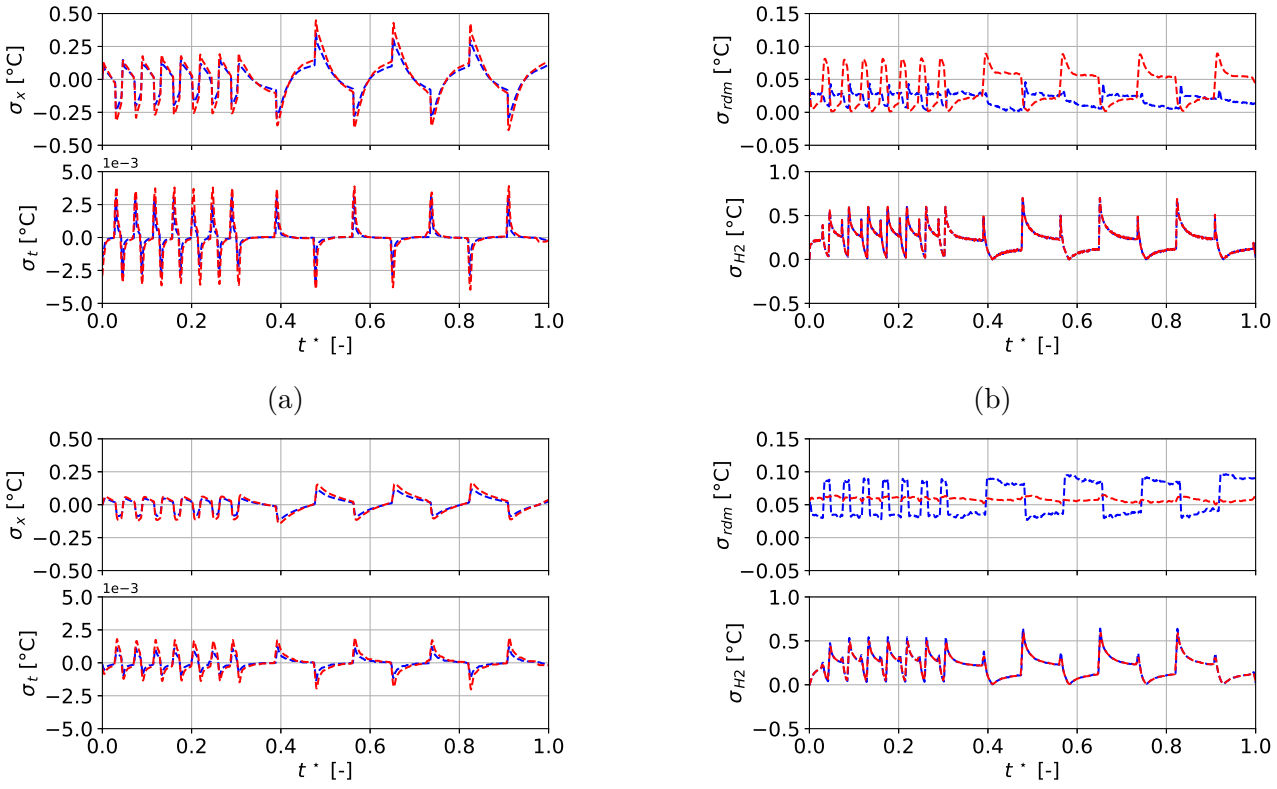


FIGURE 12 – Variation of different uncertainties on temperature at (a,b) the quarter given by $\chi_1$ (Reference) and $\chi_3$ (Reduced), (c,d) the middle given by $\chi_2$ (Reference) and $\chi_4$ (Reduced).

The calculation of uncertainties is based on the deterministic approach. In our case, this approach helps estimating the deviation in temperature or relative humidity at a given instant

and position that is caused by the largest variation of each uncertain parameter (sensor response time, surface temperature ...). This variation is expressed using the terms $\delta$, for example in Eq. (37a) and (40b). Beginning with the sensor systematic uncertainty, its value for temperature and relative humidity is already mentioned in Section 3.2. During experiments, it is assumed that the systematic accuracy do not depend on either the location or the instant of a measurement. Unlike $\sigma_{T,\mathsf{Sys}}$ and $\sigma_{\phi,\mathsf{Sys}}$, following sub-uncertainties $\sigma_{T,x}$, $\sigma_{T,t}$, $\sigma_{T,\mathsf{H2}}$, $\sigma_{\phi,x}$, $\sigma_{\phi,t}$ and $\sigma_{\phi,\mathsf{H2}}$ depend on that and are assessed numerically. To do so, the solver *Comsol Multiphysics*, which is based on finite elements method [44, 45], is used. The number of space nodes is set for both configurations to 500. As for the time step, it is set to $\Delta t_{ref} = 1\,[\mathsf{min}]$ for the reference configuration. Hence, the one related to the reduced configuration is obtained by applying similarity which leads to $\Delta t_{red} = \Delta t_{ref}\,\Sigma^2 = 0.56\,[\mathsf{min}]$. Additionally, the resolution of $\sigma_{T,\mathsf{H2}}$ and $\sigma_{\phi,\mathsf{H2}}$ requires complementary data which are surface temperature and relative humidity. These are recorded each five minutes by a sensor (Section 3.2) and included in the simulation (Section 4.5) using spline interpolations. Finally, $\sigma_{T,\mathsf{Rdm}}$ and $\sigma_{\phi,\mathsf{Rdm}}$ were approximated by using $N = 3\,[-]$ samples in each configuration (assumption 8). Ideally, the calculation of the random uncertainty is more accurate if the number $N$ is larger. In this case, the consideration of this uncertainty requires to perform the experiments related to both configurations on a large number of samples. Three samples are experimented per configuration on the basis of the six samples, that were manufactured for the study. Thus, $\sigma_{T,\mathsf{Rdm}}$ and $\sigma_{\phi,\mathsf{Rdm}}$ are evaluated in order to obtain an approximate order of magnitude with regard to other uncertainties.

Figure 12 plots the variation in uncertainties on temperature $\sigma_{T,x}$, $\sigma_{T,t}$, $\sigma_{T,\mathsf{Rdm}}$ and $\sigma_{T,\mathsf{H2}}$ at the quarter and the middle in both configurations. Firstly, two phases of variations are noticed. The first one, with high frequency, corresponds to the stress cycles that have a small time period. While the second, with a low frequency, refers to the moisture stress phase with a large period. Focusing on the uncertainty related to sensor position and the one due to sensor time response, it is worth noting that at the quarter, they are greater in reduced configuration with values ranging from 0 to 0.43 °C for $\sigma_{T,x}$ and from 0 to 0.004 °C for $\sigma_{T,t}$. This is due to the fact that the uncertainty on a sensor position regarding the reference thickness is smaller than the one with regard to the reduced thickness. Otherwise, the following relation is verified :

$$\frac{\delta_{x,ref}}{L_{ref}} < \frac{\delta_{x,red}}{L_{red}}\,. \tag{42}$$

Same logic is adopted for $\sigma_{T,t}$ when addressing the response time of a sensor and the duration of both experiments, $t_{ref}$ and $t_{red}$, instead of the uncertainty on a sensor position and thicknesses. Afterwards, it is also observed that $\sigma_{T,\mathsf{Rdm}}$ is greater at the quarter in reduced configuration with maximal values reaching 0.09 °C. However, the interpretation of this finding is not related to both sample thickness or experiment duration. It is rather due to the reproductibility of both tests. Indeed, the order of magnitude of $\sigma_{T,\mathsf{Rdm}}$ depends only on the variability of thermal properties around positions of measurement considering three samples in each configuration. The fact that this sub-uncertainty, at the quarter, is more significant in reduced configuration means that the standard deviation of thermal properties is larger around $\chi_3$ than $\chi_1$. Finally, $\sigma_{T,\mathsf{H2}}$ is also estimated, it is the largest sub-uncertainty which reached 0.7 °C. Additionally, negligible discrepancies are obtained regarding both configurations. Indeed, air temperature related to the reference and reduced configuration coincide closely in the dimensionless domain which is due to similarities.

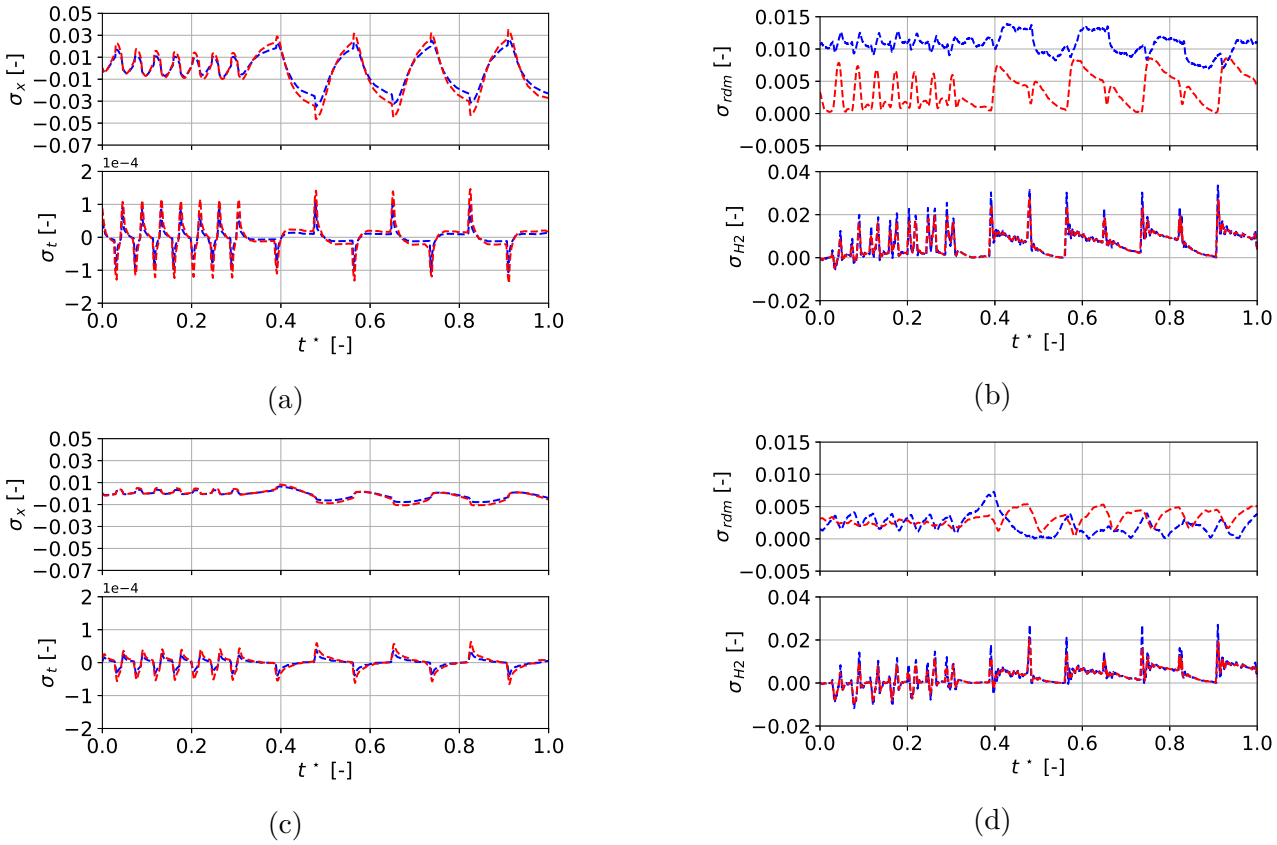


FIGURE 13 – Variation of different uncertainties on relative humidity at (a,b) the quarter given by $\chi_1$ (Reference) and $\chi_3$ (Reduced), (c,d) the middle given by $\chi_2$ (Reference) and $\chi_4$ (Reduced).

On the other hand, quite same results are noticed at the middle for both configurations. $\sigma_{T,x}$ and $\sigma_{T,t}$ are still higher in the reduced configuration. They reach peaks of about 0.16 °C and 0.002 °C, respectively. Secondly, the variation in $\sigma_{T,\mathsf{H2}}$ for both configurations is almost identical following the same reason as for $\chi_{ref,a}$ and $\chi_{red,a}$. Contrary to the result regarding $\sigma_{T,\mathsf{Rdm}}$ at the quarter, it reaches larger values in the reference configuration when focusing on the middle. This means that the variability of thermal properties around $\chi_{ref,b}$ is large. This is due to the random aspect related to a material micro-structure and pore distribution. Last, note that $\sigma_{T,x}$, $\sigma_{T,t}$ and $\sigma_{T,\mathsf{H2}}$ are smaller when getting away from the surface $x = 0$, i.e. the variation magnitude in temperature is smaller when approaching the surface bottom, where an adiabatic condition is set. Thus, the magnitude of temperature derivatives according to space, time and surface temperature is smaller when approaching the surface bottom.

In parallel, a study of uncertainties on relative humidity is also performed. Figure 13 represents the variation in uncertainties on relative humidity [1]. At the quarter, $\sigma_{\phi,x}$ and $\sigma_{\phi,t}$ vary more significantly in the reduced configuration with peaks around 0.05 and $1.4\,10^{-4}$ respectively. In addition, $\sigma_{\phi,\mathrm{Rdm}}$ informs about the variability of moisture properties around a position of measurement for a given number of samples. Considering three samples for each

1. To avoid any confusion, the results are presented in absolute value and not percentage (of vapor pressure according to saturation one) since the latter could be confusing with relative uncertainties.

configuration, the variability is larger around $\chi_{ref,a}$ where a maximum of 0.014 is remarked. Finally, the variation range of $\sigma_{\phi,\mathrm{H2}}$ at a given position does not depend on a configuration since it involves air temperature. It is about 0.03 as maximum at the quarter. Indicatively, the most dominant sub-uncertainty regarding relative humidity is the one related to sensor position.

As for the middle, it is shown that the uncertainties $\sigma_{\phi,x}$ and $\sigma_{\phi,t}$ were more important in the reduced configuration. Likewise, the uncertainty related to the modeling of boundary conditions varies little when comparing both configurations. As for $\sigma_{\phi,\mathrm{Rdm}}$, it is relatively larger in reduced configuration, which means that the variability of moisture properties is larger around $\chi_{red,b}$ than around $\chi_{ref,b}$. The influence of a position on a calculated uncertainty can also be relevant. Indeed, when considering the material in reduced configuration, notice that the magnitude of the sub-uncertainties $\sigma_{\phi,x}$, $\sigma_{\phi,t}$ and $\sigma_{\phi,\mathrm{H2}}$ is smaller at $\chi_{red,b}$ with peaks around 0.01, $5\,10^{-5}$ and 0.0275 respectively. This is due to the fact that $\chi_{red,b}$ is more distant than $\chi_{red,a}$ from areas with high temperature gradients.

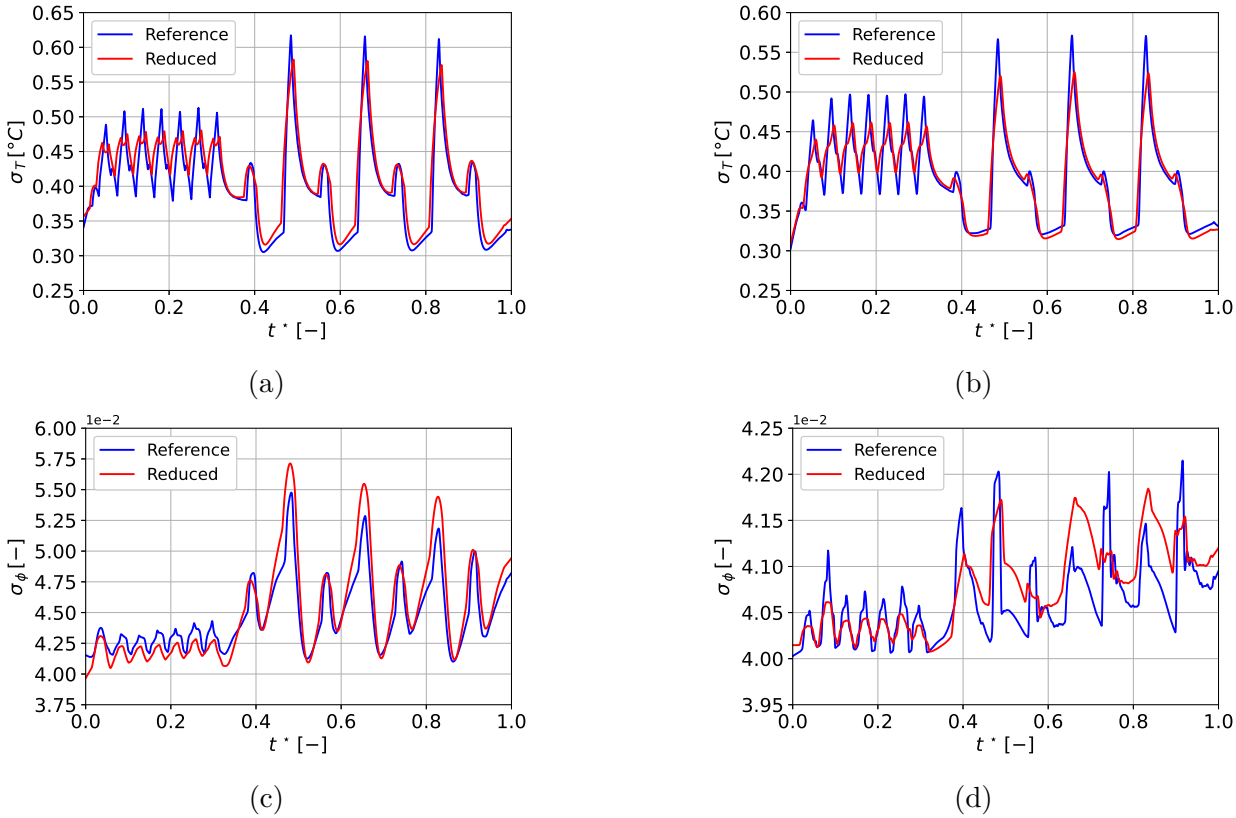


FIGURE 14 – Uncertainty on temperature and relative humidity for both configurations at $\chi_{ref,a}$ and $\chi_{red,a}$ (a,c), $\chi_{ref,b}$ and $\chi_{red,b}$ (b,d).

Figure 14 shows the variation in the entire uncertainty on temperature and relative humidity at the quarter comparing $\chi_{ref,a}$ and $\chi_{red,a}$ and the middle considering $\chi_{ref,b}$ and $\chi_{red,b}$. Remark that $\sigma_T$, at the quarter of the material in both configurations, is slightly larger than the one at the middle with maximums of 0.62 °C and 0.53 °C respectively. The same comment can be made in regard to $\sigma_\phi$ where a maximum of about 0.0575 is observed for the material quarter against 0.042 for the middle. Based on these results, two major results can be deduced.

The entire uncertainty in temperature or relative humidity is more significant in the reduced configuration. This is mainly due to the fact that the relative uncertainty on the position of the sensor and the one related to its time of response (with a lower contribution) are larger in this configuration as shown in Eq. (42) for example. Moreover, a second result is to mention. The uncertainty on relative humidity is larger at the quarter of the material than at its middle. Indeed, the position at the quarter is closer to areas with significant moisture gradients, while the middle is more distant.

Thereafter, entire uncertainties (Figure 14) are then used to calculate the confidence intervals in temperature and relative humidity as defined in Eqs. (33a) and (33b). Additionally, the magnitude of each sub-uncertainty is important in order to discuss the validity of similarity on heat and moisture diffusion. In other words, the upcoming comparison, carried out on temperature and relative humidity between both configurations, is based on the results of uncertainty. Next Section discusses the experimental results of heat and moisture similarity.

### 5.2.2 Discussion of the validity of heat and moisture diffusion similarity

Figure 15 illustrates the variation in temperature and relative humidity at the quarter and the middle of the material in both configurations. The variation is periodic where two temporal sequences are distinguished. The first part with a high frequency and the second with a low one. This observation is related to the nature of the stress scenario as explained in the previous Section. Regarding temperature at $\chi_{ref,a}$ and $\chi_{red,a}$, it varies in the same way, ranging between 22.6 and 23.75 °C approximately. In addition, slight discrepancies are observed around the peaks of curves. However, they are relatively higher when comparing temperature at the middle between both configurations ($\chi_{ref,b}$ and $\chi_{red,b}$). It reaches maximums around curve peaks of about 0.25 °C. Generally, results in temperature highlight an acceptable agreement.

Same figure shows the variation in relative humidity at the quarter and middle of the material in the reference and reduced configuration. The curves vary following two sequences while showing a good agreement especially the ones associated to $\chi_{ref,a}$ and $\chi_{red,a}$. Considering the mentioned positions, a considerable variation is observed during the second sequence where values range from 0.38 up to 0.66. Contrary to temperature, discrepancies on relative humidity between reference and reduced configuration are more significant, particularly when air relative humidity changes from 0.33 to 0.75 and vice versa. At the middle, the variation is less significant where relative humidity at $\chi_{ref,b}$ and $\chi_{red,b}$ ranges from 0.43 to 0.6. Moreover, a remarkable dephasing is illustrated when comparing relative humidity at middles. It could be caused by a difference in micro-structure between areas around $\chi_2$ and $\chi_4$. In order to evaluate discrepancies in relative humidity and its distribution, the Kernel density of probability is plotted in Fig 16.

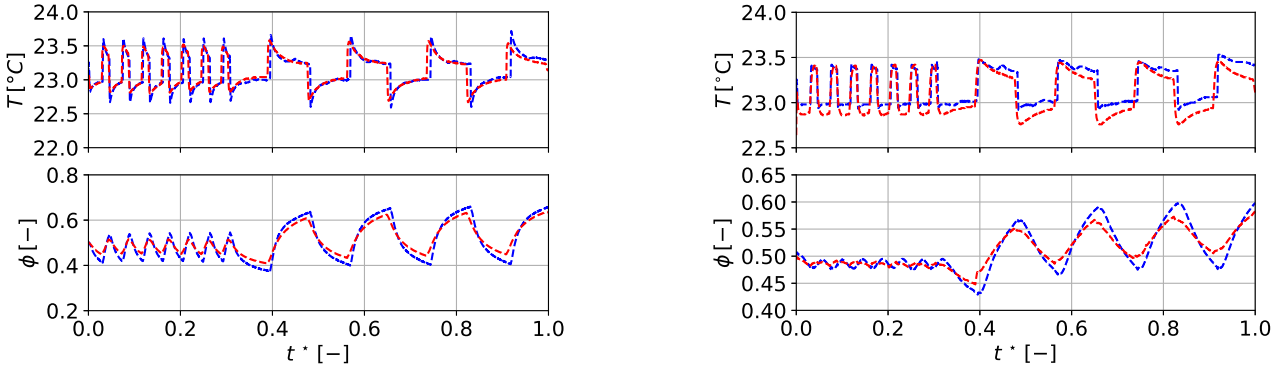


(a) (b)

FIGURE 15 – Variation in temperature and relative humidity for both configurations at (a) $\chi_{ref,a}$ and $\chi_{red,a}$, (b) $\chi_{ref,b}$ and $\chi_{red,b}$.

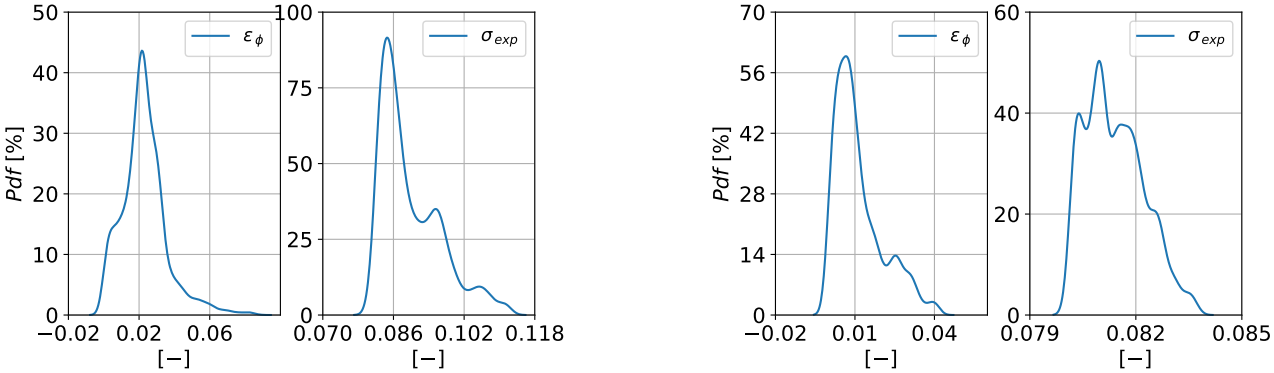


(a) (b)

FIGURE 16 – Distribution of the discrepancy on relative humidity for both configurations and the sum of the corresponding uncertainties at (a) $\chi_{ref,a}$ and $\chi_{red,a}$, (b) $\chi_{ref,b}$ and $\chi_{red,b}$.

It highlights the distribution of discrepancies on relative humidity between configurations. It is worth noting that it reaches higher values when it is evaluated at the quarter. According to Figure 16, the discrepancy can go up to 0.05 with a probability less than 5 %. In addition, the probability reaches its maximum for values around 0.02. Furthermore, the discrepancy on relative humidity is relatively smaller at the middle. It reaches a maximum of 0.035 for a probability of about 5 % and is largely around 0.007 for a probability of 60 %. Based on this comparison, it is deduced that the discrepancy between both configurations is larger if positions of measurement are close to areas with high stress gradients. This is evidenced via Figure 16, the discrepancy at the quarter is two times larger than the one at the middle. However, there is less discrepancy if the positions of measurement are more distant from areas under intense stress, as relative humidity varies slower when increasing distance.

Obtained discrepancies on temperature and relative humidity have to be discussed by considering the uncertainties at $\chi_{ref,a}$, $\chi_{ref,b}$, $\chi_{red,a}$ and $\chi_{red,b}$ as shown in Figure 14. Otherwise, confidence intervals [46, 47], as given in Eqs. (33a) and (33b), must be evaluated during the entire experiment.

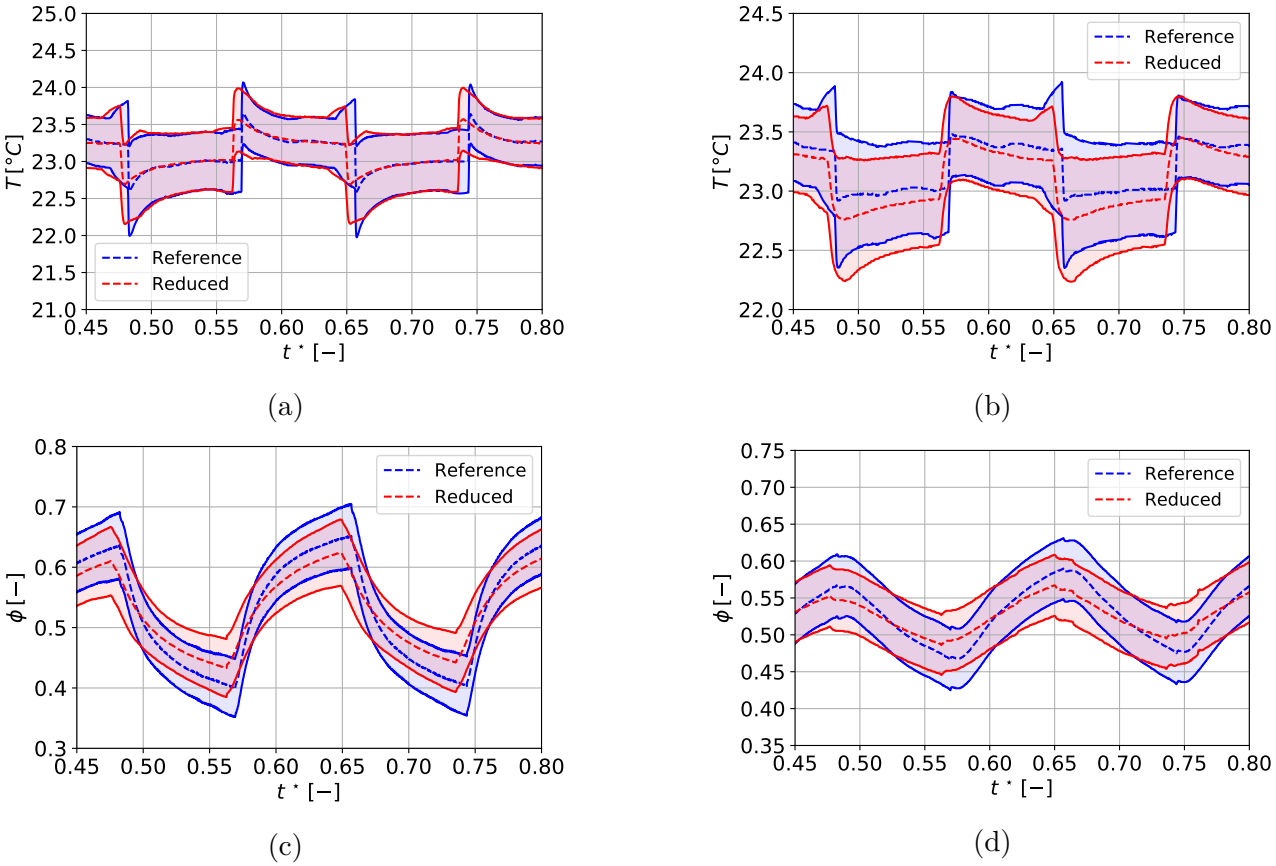


FIGURE 17 – Temperature and relative humidity variation at $\chi_{ref,a}$, $\chi_{red,a}$ (a,c) and $\chi_{ref,b}$, $\chi_{red,b}$ (b,d) with the associated confidence intervals.

Figure 17 illustrates the confidence intervals associated to temperature and relative humidity at $\chi_{ref,a}$, $\chi_{ref,b}$, $\chi_{red,a}$ and $\chi_{red,b}$ during a given sequence. The dotted lines represent the measured data, also considered as averages. Additionally, colored areas, which are delimited by two continuous lines, indicate a confidence interval, using blue for the reference positions and red for the reduced configuration. It is important noting that for two equivalent positions, significant areas are noticeable where the confidence intervals coincide. In particular, when comparing temperatures at the quarter and relative humidity at the middle. In this respect, measurements are quite comparable between the configurations with the occurrence of considerable discrepancies, mainly in relative humidity.

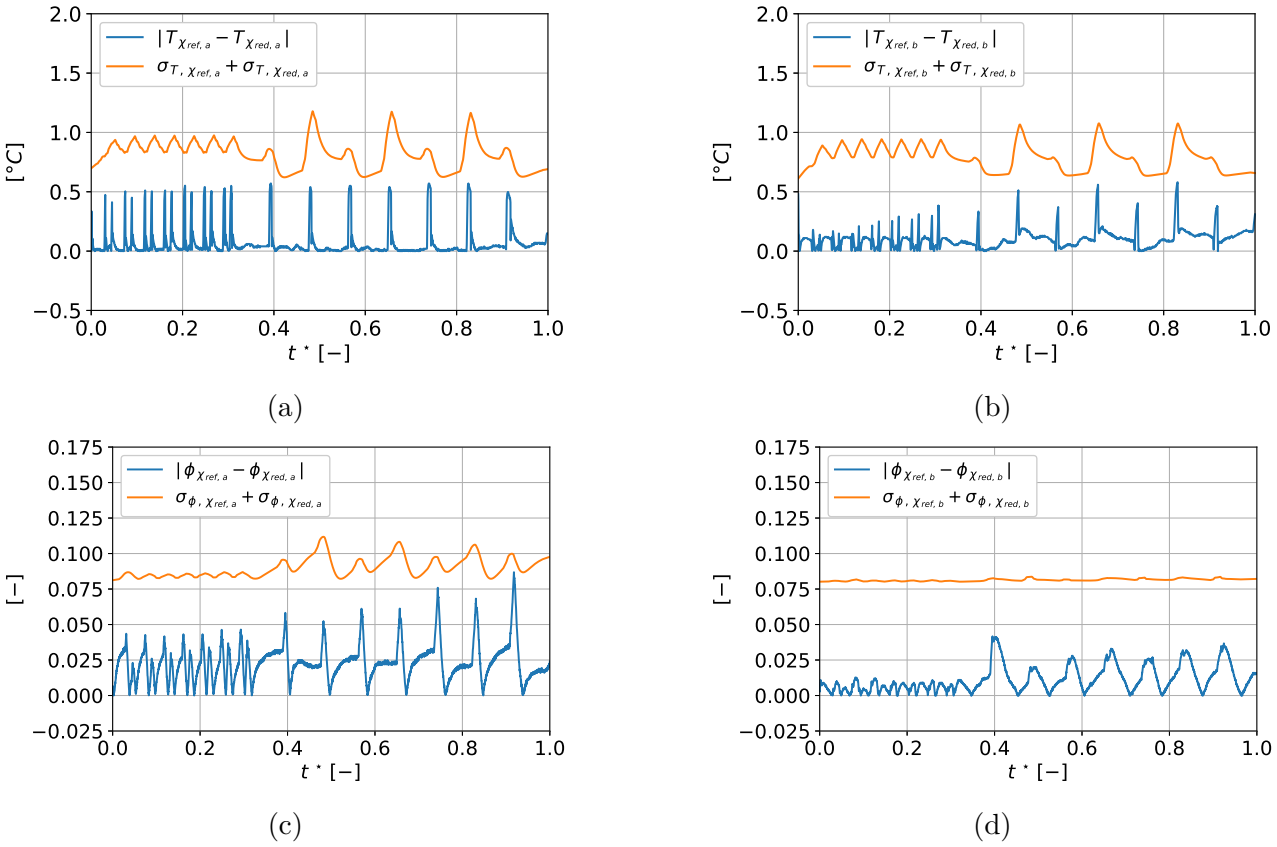


FIGURE 18 – Discrepancies on temperature and relative humidity between the reference and reduced configurations compared to the sum of the corresponding uncertainties at the quarter (a,c) and the middle (b,d).

Figure 18 helps to evaluate the magnitude of discrepancies and hence, verify entirely the conditions expressed in Eqs. (27a) and (27b). At the quarter, the discrepancy on temperature is almost 0 with oscillations up to 0.5 °C. As for relative humidity, it is larger with a maximum of about 0.075. Despite its magnitude, the discrepancy remains smaller than the uncertainty which reaches 1.2 °C and 0.11 on temperature and relative humidity respectively. Focusing on the middle, the discrepancy in temperature reaches as well 0.5 °C as a maximum, while it is less significant in relative humidity than at the quarter with 0.04 as maximum. In this case, uncertainties are also larger than discrepancies, with peaks of 1 °C and 0.08 on temperature and relative humidity respectively. After this supplementary investigation, the conditions in Eqs. (27a) and (27b) are confirmed considering $\chi_1$ and $\chi_2$ and the entire duration of both configurations. Therefore, based on the results in Figure 18, similarity of heat and moisture diffusion investigations are verified experimentally considering the two configurations defined in the study. This can also be evidenced by comparing the distribution of discrepancies with the sum of uncertainties, as shown in Figure 16. The resulting discrepancies are justified by carrying out a parallel investigation that takes into account five different sources of uncertainties.

## 5.3 Discussion and further remarks

Based on the results of the previous section, the discrepancies reached significant thresholds during several sequences. Indeed, several source errors are difficult to reduce because of certain

experimental constraints. The inaccuracy of used equipment for the two similarity experiments is a first source of error. Indeed, the ambient conditions in the climate chamber are not perfectly regulated especially relative humidity because of the size of this facility and its high inertia. As a result, air temperature and relative humidity are exposed to a margin of error. Moreover, the preconditioning of the material in relative humidity may not be completely ensured, which is caused by the high heterogeneity of its micro-structure and the presence of closed pore networks. Nevertheless, the causes previously identified, which reflect the relativity of this type of experiment, can be improved.

The results related to both configurations can also be improved. This requires a better control of the experimental conditions, i.e. an accurate verification of the assumptions set in the physical model. Considering the assumption 1, which implies that the flux is along a single direction, namely the $x$ axis. This statement is theoretical and was verified experimentally within an acceptable error [48]. Indeed, the flux is one-dimensional if the thermal conductivity of the insulator is very high compared to the one of the used material or if the latter is a semi-infinite medium along $y$ and $z$ axes. Thus, two additional sub-uncertainties $\sigma_{T,1D}$ and $\sigma_{\phi,1D}$ could have been added to address the relativity of this assumption during both similarity experiments. Ideally, its evaluation at a given coordinate $x = \chi$ is based on the measurement of temperature $T$ and relative humidity $\phi$ at all positions which have the same $x$ coordinate. This uncertainty in temperature and relative humidity is formulated as follows :

$$\sigma_{T,1\mathsf{D}}(\chi, t) = \lim_{N\to+\infty} \left( \frac{1}{N(N-1)} \sum_{i=1}^{N} (T_i - \bar{T})^2 \right)^{0.5}, \tag{43a}$$

$$\sigma_{\phi,1\mathsf{D}}(\chi, t) = \lim_{N\to+\infty} \left( \frac{1}{N(N-1)} \sum_{i=1}^{N} (\phi_i - \bar{\phi})^2 \right)^{0.5}. \tag{43b}$$

$N$ represents the number of sensors inside the material along the $y$-axis while fixing the $x$ coordinate. As remarked, the assessment of this uncertainty is definitely accurate if $N$ is infinite. However, given experimental constraints, it is quite challenging to set up a high number of sensors along a single direction. $\bar{T}$ and $\bar{\phi}$ represent the mean values at a position $\chi$, while considering variations along $y$ and $z$ axes, they are given in Eqs. (44a) and (44b) respectively :

$$\bar{T}(\chi, t) = \lim_{N\to+\infty} \frac{1}{N} \sum_{i=1}^{N} T_i, \tag{44a}$$

$$\bar{\phi}(\chi, t) = \lim_{N\to+\infty} \frac{1}{N} \sum_{i=1}^{N} \phi_i. \tag{44b}$$

In [22], authors tried to estimate this uncertainty in the framework of a heat diffusion experiment. The determination of this quantity was limited to some positions on the same plane that is defined by $x$ and $y$ axes. Values ranging from 0 to 0.1 °C were obtained for the middle of a hemp concrete sample, while applying a stress ranging from 11 to 39 °C. Thus, the uncertainty on the one-dimensional diffusion would probably be considered negligible in our study.
Otherwise, the application of similarity can be extended to three-dimensional heat and moisture diffusion. Assume that the material is used without insulation, moisture and heat flux propagate in all directions. In this respect, the physical model and its dimensionless formulation are

written while introducing two additional dimensions $L_y$ and $L_z$. Consequently, besides the coefficients $\delta$, $\gamma$ and $\eta$, four additional Fourier numbers $\mathrm{Fo_{q,y}}$, $\mathrm{Fo_{q,z}}$, $\mathrm{Fo_{m,y}}$ and $\mathrm{Fo_{m,z}}$ would be obtained. These are expressed according to Eqs. (45a) and (45b). In this case, the same factor of proportionality $\Sigma$ is used for $L_y$ and $L_z$ to obtain an equivalent configuration.

$$\mathrm{Fo}_{q,y} = \frac{\lambda_0 t_f}{\rho_{s0} C_{p0} L_y^2} \quad , \quad \mathrm{Fo}_{q,z} = \frac{\lambda_0 t_f}{\rho_{s0} C_{p0} L_z^2} , \tag{45a}$$

$$\mathrm{Fo}_{my} = \frac{k_{m0} t_f}{\rho_{s0} C_{m0} L_y^2} \quad , \quad \mathrm{Fo}_{mz} = \frac{k_{m0} t_f}{\rho_{s0} C_{m0} L_z^2} . \tag{45b}$$

A second assumption was considered in the diffusion model which is the modeling of the boundary conditions at the exposed surface using Dirichlet. This implies that air has no heat or moisture resistance, hence air temperature and relative humidity and the ones at $x = 0$ are equal. In reality, convective fluxes exist at the interacting surface which are due to the heat and water vapor coefficients $h_c$ and $h_m$. In this respect, Robin boundary conditions are the most adequate. Considering these two coefficients in the model would lead to the introduction of the Biot numbers as defined in Eq. (30). As a result, the equivalence between configurations requires an additional condition on $h_c$ and $h_m$ expressed as follows :

$$h_{c1} L_1 = h_{c2} L_2 \quad , \quad h_{m1} L_1 = h_{m2} L_{21} . \tag{46}$$

In order to ensure a similarity, it is necessary to estimate the convective coefficients associated to both configuration. However, the assessment of these coefficients relies on the knowledge of certain parameters, i.e. air physical properties, the geometry of the problem and especially air flow velocity. In the literature, empirical models were developed in fluid dynamics to estimate these coefficients, although they are limited. The reason is the experimental conditions that are different from one study to another. Consequently, the estimation of $h_c$ and $h_m$ could be possible if a correlation, proper to our experimental design, exists between these coefficients and air velocity. In this regard, the adjustment of air velocity during a configuration would help control heat and moisture convective coefficients. This might represent an experimental constraint if the climatic chamber operates at a constant air flow rate. Indeed, varying these coefficients to study the reduced configuration would not be possible, even-though their values are assumed known for the reference configuration. As a result, the verification of similarity, while using the Robin type, would rely on the realization of an experimental bench which monitors the temperature, relative humidity and air velocity.

The latter requires that properties and their laws of variation are identical between configurations. This implies that the sample micro-structure in the reduced model is similar to the one in the reference configuration.

# 6 Conclusion

Similarity laws may constitute an efficient approach to reduce the duration of a heat and moisture diffusion experiment. In this work, similarity on these coupled phenomena is experimentally assessed. In this respect, two major limitations are considered during experiments. It is assumed that heat and moisture transfer are one-dimensional. Moreover, Dirichlet boundary conditions are taken into account at the exposed material surface. A first configuration denoted

reference is proposed and defined by a 10 cm thick hemp concrete sample that is exposed to a constant temperature and a variable moisture stress during 11.5 d. As for boundary conditions, material-air interactions occur by means of a single surface. Other surfaces are considered adiabatic against heat and water vapor fluxes. To obtain the reduced configuration, a factor of proportionality 0.75 is considered. Hence, the deduced configuration involves a reduced material thickness 7.5 cm and a shorter test duration 6.47 d. To discuss similarity, temperature and relative humidity are compared at the quarter and middle of the material during both experiments. Regarding temperature, the discrepancies at the quarter and middle have the same of magnitude. As for relative humidity, the curves show a good agreement. Meanwhile, discrepancies are more relevant at the quarter than at the middle. Afterwards, the validity of similarity is tested by proposing a detailed investigation which aims, on the one hand, at evaluating the uncertainties associated to both configurations and on the other, to compare the magnitude of discrepancy with uncertainty on temperature and relative humidity.

In addition, five sub-uncertainties are proposed and defined using the deterministic approach. Results showed that for the quarter of the material, the uncertainty on temperature related to the assumption on Dirichlet boundary conditions is the dominant. As for relative humidity, the uncertainty at the quarter and related to the sensor position is the most prevalent. It is worth noting that the entire uncertainty is more significant in the reduced configuration. Finally, the validity of similarities is rigorously investigated by comparing the combined entire uncertainties of both configurations with the calculated discrepancies. Based on the latter, it is agreed that similarity on heat and moisture diffusion can be correctly applied for building materials. The verification of these laws on hemp concrete can help in future works to address scientific issues such as the investigations of material aging. It is a slow kinetic phenomenon which induces variation in material properties with time. Similarities would be employed to approach phenomena in the framework of a reduced duration experiment.

# Acknowledgments

The Region and the European Union support the project <CPER-FEDER Bâtiment durable Axis 2 MADUR Project : High-performance building materials with low environmental impact, sustainable and resilient> within the framework of the « Operational Program FEDER/FSE 2015-2020 and Energy saving certificate program of the Ministry of Ecological and Solidarity Transition "SmartReno support" 2019-2021.

# Appendix

# 1 Sensitivity study in regard to surface temperature and relative humidity

This section focuses on the sensitivity study [49, 50, 51] of heat and mass transfer model to both surface temperature and relative humidity. This is necessary in order to evaluate the partial derivatives defined in Eqs. (41). Following this, we perform a derivation of Eqs. (1), (2) (13), (14) and (15) according to surface temperature and vapor pressure. The derivation of Eq. (2) induces the following :

$$C_p\,\rho_s\,\frac{\partial\theta_1}{\partial t} = \frac{\partial}{\partial x}\left(\lambda_{ef}\,\frac{\partial\theta_1}{\partial x} + \frac{\partial\lambda_{ef}}{\partial T_s}\,\frac{\partial T}{\partial x} + \alpha\,\frac{\partial\Psi_2}{\partial x} + \frac{\partial\alpha}{\partial T_s}\,\frac{\partial P_v}{\partial x}\right). \tag{47}$$

$$C_p\,\rho_s\,\frac{\partial\Psi_1}{\partial t} = \frac{\partial}{\partial x}\left(\lambda_{ef}\,\frac{\partial\Psi_1}{\partial x} + \frac{\partial\lambda_{ef}}{\partial P_{vs}}\,\frac{\partial T}{\partial x} + \alpha\,\frac{\partial\theta_2}{\partial x} + \frac{\partial\alpha}{\partial P_{vs}}\,\frac{\partial P_v}{\partial x}\right). \tag{48}$$

Where $\theta_1$, $\theta_2$, $\Psi_1$ and $\Psi_2$ are variables depending on space and time. $\Psi_1$ is defined as follows :

$$\Psi_1(x,t) = \frac{\partial T}{\partial P_{vs}}. \tag{49}$$

They define the temperature sensitivity variables within the material regarding surface temperature and vapor pressure respectively. Additionally, $\theta_2$ and $\Psi_2$ are also sensitivity variables in this case. They represent the derivatives of the vapour pressure regarding the surface vapor pressure and temperature respectively. The are given by Eq. (50) :

$$\theta_2(x,t) = \frac{\partial P_v}{\partial P_{vs}}, \qquad \Psi_2(x,t) = \frac{\partial P_v}{\partial T_s}. \tag{50}$$

This time, we derive the second equation of the physical model according to the vapor pressure and surface temperature respectively. This operation allows us to obtain the Equations (51) and (52) :

$$\begin{aligned} C_m\,\rho_s\,\frac{\partial\theta_2}{\partial t} + \rho_s\,\frac{\partial C_m}{\partial P_{vs}}\,\frac{\partial P_v}{\partial t} = \frac{\partial}{\partial x}\left(k_m\,\frac{\partial\theta_2}{\partial x} + \frac{\partial k_m}{\partial P_{vs}}\,\frac{\partial P_v}{\partial x} + k_T\,\frac{\partial\Psi_1}{\partial x} + \frac{\partial k_T}{\partial P_{vs}}\,\frac{\partial T}{\partial x}\right)+ \\ \beta\,\frac{\partial\Psi_1}{\partial t} + \frac{\partial\beta}{\partial P_{vs}}\,\frac{\partial T}{\partial t}. \end{aligned} \tag{51}$$

$$\begin{aligned} C_m\,\rho_s\,\frac{\partial\Psi_2}{\partial t} + \rho_s\,\frac{\partial C_m}{\partial T_s}\,\frac{\partial P_v}{\partial t} = \frac{\partial}{\partial x}\left(k_m\,\frac{\partial\Psi_2}{\partial x} + \frac{\partial k_m}{\partial T_s}\,\frac{\partial P_v}{\partial x} + k_T\,\frac{\partial\theta_1}{\partial x} + \frac{\partial k_T}{\partial T_s}\,\frac{\partial T}{\partial x}\right)+ \\ \beta\,\frac{\partial\theta_1}{\partial t} + \frac{\partial\beta}{\partial T_s}. \end{aligned} \tag{52}$$

Equations (47), (48), (51) and (52) include terms related to the influence of a surface temperature or vapor pressure variation on material thermal and moisture properties. These terms are non-zero because model parameters depend on both material thermal and hydric states. Starting with moisture storage capacity $C_m$ , its derivatives according to surface temperature and vapor pressure are given by Eqs. (53) and (54) :

$$\frac{\partial C_m}{\partial T_s} = -\frac{1}{P_{sat}^2}\,\frac{\partial P_{sat}}{\partial T}\,\theta_1\left(\frac{\partial\omega}{\partial\phi} + \phi\,\frac{\partial^2\omega}{\partial\phi^2}\right) + \frac{\Psi_2}{P_{sat}^2}\,\frac{\partial^2\omega}{\partial\phi^2}, \tag{53}$$

$$\frac{\partial C_m}{\partial P_{vs}} = -\frac{1}{P_{sat}^2}\frac{\partial P_{sat}}{\partial T}\Psi_1\Big(\frac{\partial \omega}{\partial \phi} + \phi\frac{\partial^2 \omega}{\partial \phi^2}\Big) + \frac{\theta_2}{P_{sat}^2}\frac{\partial^2 \omega}{\partial \phi^2}\,. \tag{54}$$

Secondly, the derivative of the total mass permeability $k_m$ according to $T_s$ and $P_{vs}$ are given as follows :

$$\frac{\partial k_m}{\partial T_s} = \frac{\partial k_m}{\partial \phi}\frac{\partial \phi}{\partial T}\theta_1, \qquad \frac{\partial k_m}{\partial P_{vs}} = \frac{1}{P_{sat}}\frac{\partial k_m}{\partial \phi}\theta_2\,. \tag{55}$$

The derivative of the total mass permeability according to relative humidity in Eq. (55) is estimated based on experimental data. Precisely, this data describe the evolution of $k_m$ according to $\phi$ inside the material. Subsequently, the coefficient $k_T$ depend also on temperature and vapor pressure as demonstrated in Eq. (8). Thus, its derivatives are obtained according to Eqs. (56) and (57) :

$$\frac{\partial k_T}{\partial T_s} = \frac{R\,\rho_l}{M}\Big[\frac{k_l\,R\,\rho_l}{M\,P_v}\theta_1\Big(T\frac{\partial \ln\,\phi}{\partial T} + \ln\,\phi\Big) + k_l\Big(\theta_1\frac{\partial \ln\,\phi}{\partial T} + T\frac{\partial}{\partial T}\Big(\frac{\Psi_2}{P_v} - \frac{\theta_1}{P_{sat}}\frac{\partial P_{sat}}{\partial T}\Big) + \frac{\Psi_2}{P_v} - \frac{\theta_1}{P_{sat}}\frac{\partial P_{sat}}{\partial T}\Big)\Big]\,. \tag{56}$$

$$\frac{\partial k_T}{\partial P_{vs}} = \frac{R\,\rho_l}{M}\Big[\frac{k_l\,R\,\rho_l}{M\,P_v}\Psi_1\Big(T\frac{\partial \ln\,\phi}{\partial T} + \ln\,\phi\Big) + k_l\Big(\Psi_1\frac{\partial \ln\,\phi}{\partial T} + T\frac{\partial}{\partial T}\Big(\frac{\theta_2}{P_v} - \frac{\Psi_1}{P_{sat}}\frac{\partial P_{sat}}{\partial T}\Big) + \frac{\theta_2}{P_v} - \frac{\Psi_1}{P_{sat}}\frac{\partial P_{sat}}{\partial T}\Big)\Big]\,. \tag{57}$$

Moreover, the coefficient $\beta$ is the last one in mass conservation Eq. (1) that varies according to temperature and vapor pressure. Its derivatives regarding these two variables are expressed following Eqs. (58) and (59) :

$$\frac{\partial \beta}{\partial T_s} = \Big(\frac{\rho_s\,C_m}{P_{sat}}\frac{\partial P_{sat}}{\partial T} + \frac{\rho_s\,P_v}{P_{sat}^3}\frac{\partial^2 \omega}{\partial \phi^2}\frac{\partial P_{sat}}{\partial T}\Big)\Psi_2\,. \tag{58}$$

$$\frac{\partial \beta}{\partial P_{vs}} = \Big(\frac{\rho_s\,C_m}{P_{sat}}\frac{\partial P_{sat}}{\partial T} + \frac{\rho_s\,P_v}{P_{sat}^3}\frac{\partial^2 \omega}{\partial \phi^2}\frac{\partial P_{sat}}{\partial T}\Big)\theta_2\,. \tag{59}$$

Finally, effective thermal conductivity and the coefficient $\alpha$ are the two varying properties considered in Eq. (2). Thus, their derivatives are obtained as follows :

$$\frac{\partial \lambda_{ef}}{\partial T_s} = \lambda_{ef}\,C_m\,\rho_l\,\rho_s\,\ln(\lambda_l)\,\Psi_2\,, \qquad \frac{\partial \lambda_{ef}}{\partial T_s} = \lambda_{ef}\,C_m\,\rho_l\,\rho_s\,\ln(\lambda_l)\,\theta_2\,. \tag{60}$$

$$\frac{\partial \alpha}{\partial T_s} = (h_l + L_v)\frac{\partial k_m}{\partial \phi}\frac{\partial \phi}{\partial T}\theta_1\,, \qquad \frac{\partial \alpha}{\partial P_{vs}} = \frac{1}{P_{sat}}(h_l + L_v)\frac{\partial k_m}{\partial \phi}\theta_2\,. \tag{61}$$

Regarding the boundary conditions, Equations expressing them given in Section 2.2 are derived according to $P_{vs}$ and $T_s$. First, we begin with Dirichlet condition given in Eq. (14). We obtain therefore $\forall\, t \in [\,0\,,\,t_f\,]$, $x = 0$ :

$$\theta_1 = 1\,, \quad \Psi_2 = 0\,. \tag{62}$$

$$\theta_2 = 1\,, \quad \Psi_1 = 0\,. \tag{63}$$

On the other hand, the boundary conditions in the Eq. (15) regarding thermal and mass flux undergo the same derivation resulting in the following where $t \in [\,0\,,\, t_f\,]$ and $x = L$ :

$$\frac{\partial \theta_1}{\partial x} = 0\,, \quad \frac{\partial \Psi_2}{\partial x} = 0\,. \tag{64}$$

$$\frac{\partial \theta_2}{\partial x} = 0\,, \quad \frac{\partial \Psi_1}{\partial x} = 0\,. \tag{65}$$

Finally, we derive Eq. (13) in order to express initial conditions regarding the variables $\theta_1$, $\theta_2$, $\phi_1$ and $\phi_2$. Therefore, we obtain :

$$\forall\, x \in [\,0\,,\, L\,]\,,\, t = 0 \qquad \theta_1 = 0\,,\, \theta_2 = 0\,,\, \Psi_1 = 0\,,\, \Psi_2 = 0\,. \tag{66}$$

To conclude, the study of the temperature and relative humidity sensitivity with regard to that at the material surface $x = 0$, allows us to evaluate the coefficients $\theta_1$, $\theta_2$, $\Psi_1$ and $\Psi_3$ by solving Eqs. (47), (48), (51) and (52). The boundary conditions corresponding to the study of sensitivity are given by Eq. (62), (63), (64) and (65). At the end, the initial conditions are represented in Eq. (66). Once the results are obtained, we deduce $\sigma_{T,\,\mathrm{H2}}$ and $\sigma_{\phi,\,\mathrm{H2}}$ considering that :

$$\begin{aligned} \theta_3 = & \left( \frac{\theta_2}{P_{sat}} - \frac{P_v}{P_{sat}^2} \frac{\partial P_{sat}}{\partial T}\, \Psi_1 \right) P_{sat}\,(\,T_s\,) - \\ & \left( \frac{\Psi_2}{P_{sat}} - \frac{P_v}{P_{sat}^2} \frac{\partial P_{sat}}{\partial T}\, \theta_1 \right) \left( \frac{\phi_s}{P_{sat}\,(\,T_s\,)} \frac{\partial P_{sat}\,(\,T_s\,)}{\partial T_s} \right)^{-1}. \end{aligned} \tag{67}$$

# Reference


[1] J. Berger, T. Busser, S. Reddy, and G. S. Dulikravich, "Evaluation of the reliability of a heat and mass transfer model in hygroscopic material," *International Journal of Heat and Mass Transfer*, vol. 142, p. 118258, 2019. [Online]. Available : https://www.sciencedirect.com/science/article/pii/S0017931019318964

[2] T. Busser, J. Berger, A. Piot, M. Pailha, and M. Woloszyn, "Comparison of model numerical predictions of heat and moisture transfer in porous media with experimental observations at material and wall scales : An analysis of recent trends," *Drying Technology*, vol. 37, no. 11, pp. 1363–1395, 2019. [Online]. Available : https://doi.org/10.1080/07373937.2018.1502195

[3] H. Rafidiarison, R. Rémond, and E. Mougel, "Dataset for validating 1-d heat and mass transfer models within building walls with hygroscopic materials," *Building and Environment*, vol. 89, pp. 356–368, 2015. [Online]. Available : https://www.sciencedirect.com/science/article/pii/S0360132315001158

[4] T. Colinart, D. Lelievre, and P. Glouannec, "Experimental and numerical analysis of the transient hygrothermal behavior of multilayered hemp concrete wall," *Energy and Buildings*, vol. 112, pp. 1–11, 2016. [Online]. Available : https://www.sciencedirect.com/science/article/pii/S0378778815303960

[5] M. Maaroufi, R. Belarbi, K. Abahri, and F. Benmahiddine, "Full characterization of hygrothermal, mechanical and morphological properties of a recycled expanded polystyrene-based mortar," *Construction and Building Materials*, vol. 301, p. 124310, 2021. [Online]. Available : https://www.sciencedirect.com/science/article/pii/S0950061821020699

[6] D. Lelievre, T. Colinart, and P. Glouannec, "Hygrothermal behavior of bio-based building materials including hysteresis effects : Experimental and numerical analyses," *Energy and Buildings*, vol. 84, pp. 617–627, 2014. [Online]. Available : https://www.sciencedirect.com/science/article/pii/S0378778814007038

[7] R. L. Thompson and E. J. Soares, "Viscoplastic dimensionless numbers," *Journal of Non-Newtonian Fluid Mechanics*, vol. 238, pp. 57–64, 2016, viscoplastic Fluids From Theory to Application 2015 (VPF6). [Online]. Available : https://www.sciencedirect.com/science/article/pii/S0377025716300465

[8] M. C. Ruzicka, "On dimensionless numbers," *Chemical Engineering Research and Design*, vol. 86, no. 8, pp. 835–868, 2008.

[9] X. Qian, Z. Liu, and J. Xu, "A scaling law for designing a downscaled model to investigate submarine debris-flow impact on a pipeline in normal gravity," *Ocean Engineering*, vol. 251, p. 111152, 2022. [Online]. Available : https://www.sciencedirect.com/science/article/pii/S0029801822005613

[10] A. Pucciarelli and W. Ambrosini, "A successful general fluid-to-fluid similarity theory for heat transfer at supercritical pressure," *International Journal of Heat and Mass Transfer*, vol. 159, 2020.

[11] S. Kassem, A. Pucciarelli, and W. Ambrosini, "Insight into a fluid-to-fluid similarity theory for heat transfer at supercritical pressure : Results and perspectives," *International Journal of Heat and Mass Transfer*, vol. 168, 2021.

[12] S. Sharma and S. K. Saha, "Development of scaling laws for prototyping and heat loss correlations for upward facing cylindrical helical coil and conical spiral coil receivers," *International Journal of Heat and Mass Transfer*, vol. 190, p. 122773, 2022. [Online]. Available : https://www.sciencedirect.com/science/article/pii/S0017931022002551

[13] L. M. Mazzariol and M. Alves, "Similarity laws of structures under impact load : Geometric and material distortion," *International Journal of Mechanical Sciences*, vol. 157-158, pp. 633–647, 2019. [Online]. Available : https://www.sciencedirect.com/science/article/pii/S0020740319304138

[14] A. Berry, O. Robin, F. Franco, S. D. Rosa, and G. Petrone, "Similitude laws for the sound radiation of flat orthotropic flexural panels," *Journal of Sound and Vibration*, vol. 489, p. 115636, 2020. [Online]. Available : https://www.sciencedirect.com/science/article/pii/S0022460X20304570

[15] B. Li, D. L. Zhou, Y. Wang, Y. Shuai, Q. Z. Liu, and W. H. Cai, "The design of a small lab-scale wind turbine model with high performance similarity to its utility-scale prototype," *Renewable Energy*, vol. 149, pp. 435–444, 2020.

[16] K. Zhang, F. Lu, Y. Peng, and X. Li, "Study on dynamic response of gravity dam under air blast load based on similarity law," *Engineering Failure Analysis*, vol. 138, p. 106225, 2022. [Online]. Available : https://www.sciencedirect.com/science/article/pii/S1350630722001996

[17] J. xi Chen, "Similarity law of flowrate for hot-gas ventilated supercavity flows," *Journal of Hydrodynamics, Ser. B*, vol. 22, no. 5, Supplement 1, pp. 852–858, 2010. [Online]. Available : https://www.sciencedirect.com/science/article/pii/S1001605810600418

[18] Q. Ai, W. Wang, Y. Gong, X. Zhang, Y. Shuai, M. Xie, and H. Tan, "Study on similarity criteria for aerodynamic/thermal coupling analysis of the aircraft," *International Communications in Heat and Mass Transfer*, vol. 129, no. October, p. 105705, 2021. [Online]. Available : https://doi.org/10.1016/j.icheatmasstransfer.2021.105705

[19] C. Zhang, J. Wei, S. Hou, and J. Zhang, "Scaling law of gear transmission system obtained from dynamic equation and finite element method," *Mechanism and Machine Theory*, vol. 159, p. 104285, 2021. [Online]. Available : https://www.sciencedirect.com/science/article/pii/S0094114X21000434

[20] Y. Zhou, S. Feng, and J. Li, "Study on the failure mechanism of rock mass around a mined-out area above a highway tunnel – similarity model test and numerical analysis," *Tunnelling and Underground Space Technology*, vol. 118, p. 104182, 2021. [Online]. Available : https://www.sciencedirect.com/science/article/pii/S0886779821003734

[21] M. Matsumoto and S. Fujiwara, "A study of annual moisture variation in an internally insulated building wall under a mild climate using a small-scale model and the similarity laws," *Energy and Buildings*, vol. 16, no. 3-4, pp. 933–945, 1991.

[22] A. Charaka, J. Berger, and R. Belarbi, "Experimental assessment of the similarity law for a heat conduction problem," *Thermal Science and Engineering Progress*, p. 101312, 2022. [Online]. Available : https://www.sciencedirect.com/science/article/pii/S2451904922001196

[23] J. Berger, C. Legros, and M. Abdykarim, "Dimensionless formulation and similarity to assess the main phenomena of heat and mass transfer in building porous material," *Journal of Building Engineering*, vol. 35, no. September 2020, p. 101849, 2021. [Online]. Available : https://doi.org/10.1016/j.jobe.2020.101849

[24] F. Kong and M. Zheng, "Effects of combined heat and mass transfer on heating load in building drying period," *Energy and Buildings*, vol. 40, no. 8, pp. 1614–1622, 2008.

[25] M. Simo-Tagne, R. Remond, R. Kharchi, L. Bennamoun, M. C. Ndukwu, and Y. Rogaume, "Modeling, numerical simulation and validation of the hygrothermal transfer through a wooden building wall in Nancy, France," *Thermal Science and Engineering Progress*, vol. 22, no. December 2020, p. 100808, 2021. [Online]. Available : https://doi.org/10.1016/j.tsep.2020.100808

[26] S. Eraslan, I. M. Gitman, H. Askes, and R. de Borst, "Determination of representative volume element size for a magnetorheological elastomer," *Computational Materials Science*, vol. 203, p. 111070, 2022. [Online]. Available : https://www.sciencedirect.com/science/article/pii/S092702562100745X

[27] S. Whitaker, *Volume Averaging of Transport Equations*, 01 1997, pp. 1–60.

[28] L. Wang, L.-P. Wang, Z. Guo, and J. Mi, "Volume-averaged macroscopic equation for fluid flow in moving porous media," *International Journal of Heat and Mass Transfer*, vol. 82, pp. 357–368, 2015. [Online]. Available : https://www.sciencedirect.com/science/article/pii/S0017931014010448

[29] T. Colinart and P. Glouannec, "Temperature dependence of sorption isotherm of hygroscopic building materials. Part 1 : Experimental evidence and modeling," *Energy and Buildings*, vol. 139, pp. 360–370, 2017. [Online]. Available : http://dx.doi.org/10.1016/j.enbuild.2016.12.082

[30] F. Bennai, M. Y. Ferroukhi, F. Benmahiddine, R. Belarbi, and A. Nouviaire, "Assessment of hygrothermal performance of hemp concrete compared to conventional building materials at overall building scale," *Construction and Building Materials*, vol. 316, no. December 2021, p. 126007, 2022. [Online]. Available : https://doi.org/10.1016/j.conbuildmat.2021.126007

[31] M. Y. Ferroukhi, K. Abahri, R. Belarbi, and K. Limam, "Integration of a hygrothermal transfer model for envelope in a building energy simulation model : experimental validation of a HAM–BES co-simulation approach," *Heat and Mass Transfer/Waerme- und Stoffuebertragung*, vol. 53, no. 6, pp. 1851–1861, 2017.

[32] A. Trabelsi, Z. Slimani, and J. Virgone, "Response surface analysis of the dimensionless heat and mass transfer parameters of Medium Density Fiberboard," *International Journal of Heat and Mass Transfer*, vol. 127, pp. 623–630, 2018. [Online]. Available : https://doi.org/10.1016/j.ijheatmasstransfer.2018.05.145

[33] B. Jamal, M. Boukendil, A. Abdelbaki, and Z. Zrikem, "Numerical simulation of coupled heat transfer through double solid walls separated by an air layer," *International Journal*

*of Thermal Sciences*, vol. 156, no. April 2018, p. 106461, 2020. [Online]. Available : https://doi.org/10.1016/j.ijthermalsci.2020.106461

[34] F. Collet, J. Chamoin, S. Pretot, and C. Lanos, "Comparison of the hygric behaviour of three hemp concretes," *Energy and Buildings*, vol. 62, pp. 294–303, 2013. [Online]. Available : http://dx.doi.org/10.1016/j.enbuild.2013.03.010

[35] F. Benmahiddine, R. Cherif, F. Bennai, R. Belarbi, A. Tahakourt, and K. Abahri, "Effect of flax shives content and size on the hygrothermal and mechanical properties of flax concrete," *Construction and Building Materials*, vol. 262, p. 120077, 2020. [Online]. Available : https://doi.org/10.1016/j.conbuildmat.2020.120077

[36] M. I. H. Khan, Z. Welsh, Y. Gu, M. A. Karim, and B. Bhandari, "Modelling of simultaneous heat and mass transfer considering the spatial distribution of air velocity during intermittent microwave convective drying," *International Journal of Heat and Mass Transfer*, vol. 153, 2020.

[37] T. Defraeye, B. Blocken, and J. Carmeliet, "Convective heat transfer coefficients for exterior building surfaces : Existing correlations and CFD modelling," *Energy Conversion and Management*, vol. 52, no. 1, pp. 512–522, 2011. [Online]. Available : http://dx.doi.org/10.1016/j.enconman.2010.07.026

[38] W. Belazi, S. E. Ouldboukhitine, A. Chateauneuf, and A. Bouchair, "Uncertainty analysis of occupant behavior and building envelope materials in office building performance simulation," *Journal of Building Engineering*, vol. 19, no. May, pp. 434–448, 2018. [Online]. Available : https://doi.org/10.1016/j.jobe.2018.06.005

[39] J. R. Taylor, "[John_R._Taylor]_An_Introduction_to_Error_Analysis(BookZZ.org).pdf," 1997.

[40] H. Sari-Sarraf, E. Delp, T. Aach, M. S. Pattichis, and J. P. Havlicek, "Engineering analysis of experimental data," vol. 986, 2004.

[41] T. Lu and C. Chen, "Uncertainty evaluation of humidity sensors calibrated by saturated salt solutions," *Measurement : Journal of the International Measurement Confederation*, vol. 40, no. 6, pp. 591–599, 2007.

[42] S. Lee, "Monte Carlo simulation using support vector machine and kernel density for failure probability estimation," *Reliability Engineering and System Safety*, vol. 209, no. November 2020, p. 107481, 2021. [Online]. Available : https://doi.org/10.1016/j.ress.2021.107481

[43] T. P. Chang, "Estimation of wind energy potential using different probability density functions," *Applied Energy*, vol. 88, no. 5, pp. 1848–1856, 2011. [Online]. Available : http://dx.doi.org/10.1016/j.apenergy.2010.11.010

[44] J. Zhang and S. Chauhan, "Fast explicit dynamics finite element algorithm for transient heat transfer," *International Journal of Thermal Sciences*, vol. 139, no. October 2018, pp. 160–175, 2019. [Online]. Available : https://doi.org/10.1016/j.ijthermalsci.2019.01.030

[45] J. Xiao, Y. Liu, J. Wanga, P. Bénard, and R. Chahine, "Finite element simulation of heat and mass transfer in activated carbon hydrogen storage tank," *International Journal of Heat and Mass Transfer*, vol. 55, no. 23-24, pp. 6864–6872, 2012. [Online]. Available : http://dx.doi.org/10.1016/j.ijheatmasstransfer.2012.06.093

[46] R. Willink and I. Lira, "A united interpretation of different uncertainty intervals," *Measurement : Journal of the International Measurement Confederation*, vol. 38, no. 1, pp. 61–66, 2005.

[47] S. Rouchier, T. Busser, M. Pailha, A. Piot, and M. Woloszyn, "Hygric characterization of wood fiber insulation under uncertainty with dynamic measurements and Markov Chain Monte-Carlo algorithm," *Building and Environment*, vol. 114, pp. 129–139, 2017.

[48] A. Charaka, J. Berger, and R. Belarbi, "Experimental assessment of the similarity law for a heat conduction problem," *En cours de soumission*, 2021.

[49] A. Jumabekova, J. Berger, A. Foucquier, and G. S. Dulikravich, "Searching an optimal experiment observation sequence to estimate the thermal properties of a multilayer wall under real climate conditions," *International Journal of Heat and Mass Transfer*, vol. 155, p. 119810, 2020. [Online]. Available : https://doi.org/10.1016/j.ijheatmasstransfer.2020.119810

[50] E. S. P. B. V, E. Sidiropoulos, and C. Tzimopoulos, "Sensitivity analysis of a coupled heat and mass transfer model in unsaturated porous media," *Science*, vol. 64, pp. 281–298, 1983.

[51] A. Gelesz, E. Catto Lucchino, F. Goia, V. Serra, and A. Reith, "Characteristics that matter in a climate façade : A sensitivity analysis with building energy simulation tools," *Energy and Buildings*, vol. 229, p. 110467, 2020. [Online]. Available : https://doi.org/10.1016/j.enbuild.2020.110467